Development of a minimalist conceptual numerical model for flood forecasting and management under GIS environment

Mustapha Rabie Boudani, Mohamed Mazour, Hichem Mazighi and Omar Djoukbala

ABSTRACT

The floods that Algeria has experienced in recent years are among the most significant natural disasters recorded by the country. These disasters, whose amplitude and frequency have tended to become increasingly irregular in space and time, in the current context of global climate change, encourage us to improve our flood management and forecasting strategies, notably through the re-evaluation of protection structure capacities, designed on the basis of hydrological data analyzed by statistical adjustment of past rainfall hazards. The objective of this study is to develop a minimalist conceptual numerical model for flood forecasting and management under GIS environment for the north-east region of Algeria. This model was developed by analyzing hydrographic data that can be adapted to climate data collected in real time, to predict short-term flood hydrographs in all segments of the hydrographic network, based on the Sokolovsky model for construction of synthetic hydrographs, combined with the Horton architecture for basin discretization. We obtained accuracy on past rainfall hazard simulations around 65.2% for peak flow amplitudes and 88.3% for surface runoff base times. This low-cost simple model opens the way to more possibilities in flood management, and can be improved through better spatialization and calibration with more field data.

Key words | Algeria, conceptual rainfall-runoff model, flood forecasting systems, flood management, flood modelling, geographic information system

Mustapha Rabie Boudani (corresponding author)
Mohamed Mazour
Omar Djoukbala
LHYDENV Laboratory,
Belhadj Bouchaib University Center of Ain Temouchent,
Ain Temouchent,
Algeria
E-mail: *b-musta@hotmail.fr*

Hichem Mazighi
Laboratoire Mobilisation et Valorisation des Ressources en Eau (MVRE),
École Nationale Supérieure d'Hydraulique (ENSH),
Blida,
Algeria

INTRODUCTION

The consequences of global warming, already palpable, will become increasingly noticeable with multiplication and intensification of floods episodes, heat and drought periods (IPCC 2007; Hirabayashi *et al.* 2013; Donat *et al.* 2016). From that perspective, it becomes crucial to reconsider a large part of flood protection structures, since they have been dimensioned by statistical adjustment of past rainfall hazard series, which may no longer be representative of future hazards, given the current climate conditions. Hence, it is necessary to rethink our flood management and forecasting methods and strategies.

Thus, in such a future, flood forecasting systems (FFS) will remain among the most effective means of flood protection. In addition to allowing flood flows prediction and flood risk areas with a significant time margin, FFS can simulate many plausible climatic hazards, while building a robust hydrological database and thus be a powerful tool in urban development. These solutions, whether conceptual, empirical, or even black box, are strictly analytical and will be more and more precise and accessible given continuous technological progress.

Even if the developed countries, which are mostly wet, have enough flood forecasting infrastructure, such as the

doi: 10.2166/wcc.2020.265

USA (USGS – NWIS 2001), France (ESPADA 2005), Switzerland (FEON – Hydrodaten 2007), Australia (WaterNSW 2014), etc., this is not the case in developing countries. Mostly arid to semi-arid, the latter, in view of their climates, have not prioritized flood control during their urban development and are equally affected by the consequences of climate change at different scales.

Anticipation and monitoring of the phenomena which generate floods requires different categories of devices and tools (CEPRI 2017), which should be distinguished as:

1. monitoring systems based on the observation of hydrometeorological phenomena;
2. monitoring systems based on weather forecasting;
3. monitoring systems based on flood flow forecasting;
4. monitoring systems based on flooding forecasting.

The model developed in this study is in the third category according to monitoring systems based on flood flow forecasting. It is a spatialized hydrological model dedicated to the forecasting of river flood flows, by regionalized calculation of rainfall-runoff transformations. It can thus only delimit floodplain areas after injecting the predicted flows into another model dedicated to hydrodynamic flow simulations.

There are several mathematical models dedicated to the calculation of flood hydrographs (calculation of the evolution of flows as a function of time resulting from given rainfall events), commonly known as hydrological models or rainfall-runoff models. The first so-called global models were developed in the early 1940s, such as the Sokolovsky unit hydrograph (Sokolovsky 1949, 1959; Sokolovsky & Shiklomanov 1969), instantaneous unit hydrograph and geomorphological instantaneous unit hydrograph (Rodríguez-Iturbe & Valdés 1979), unit hydrograph accumulation method 'summation of individual direct runoff hydrograph ∑DRHs' (Chow *et al.* 1988) and the S-curve method (Edson 1951), etc. These minimalist models, sometimes empirical, laid the foundations for predictive calculations of flood assessment and recession flows at the outlet of basins, based on an average assessment of basins' characteristics and the rainfall assumed to be uniformly distributed. Although offering generally good results, they encountered some restrictions such as limits of the spatial variability of flood governing factors (Al-Juaidi *et al.* 2018; Tehrany *et al.* 2019), thus reducing considerably their application fields. These models evolved in the 1970s, with the advent of computer devices, towards concepts of distributed calculations (more localized), known as contributory zones, such as the TOPMODEL model (Beven & Kirkby 1979; Quinn *et al.* 1995; Saulnier *et al.* 1997) and TOPODYN (Datin 1999), etc.

At the beginning of the 1990s, with the development of power computing, Information and Communications Technology (ICT) and the emergence of geographic information systems (GIS), river flow forecasts became more accessible, and of great interest to the scientific community, which led to the development of several concepts of rainfall-runoff models, and can be classified into four categories:

- Spatialized hydrological models, such as the MERSEDES model (Bouvier 1994; Bouvier *et al.* 1994), GUHR model (Agirre *et al.* 2005), ISBA-TOPMODEL (Habets & Saulnier 2001; Vincendon *et al.* 2010), etc. These conceptual models calculate the rainfall-runoff transformation, based on discretization of catchment areas into meshes, for which various factors conditioning the floods can be evaluated separately. These models require less historical rainfall and runoff data for their calibration, while offering relevant predictions. Although adaptable to wide areas, they require quality topographic data and many factors to be incorporated to condition the hydrodynamic interactions into various grids.
- Black box hydrological models (Xu *et al.* 2019), such as the antecedent precipitation index (Kohler & Linsley 1951), regression models (Riggs 1985), time series models (Salas 1980), etc. These empirical models are based on the analysis of the relations between the inputs (rain) and the outputs (flow discharge) without seeking to integrate hydrodynamic or conversion phenomena. These models therefore require a large amount of historical rainfall and flow data for their calibration and are built around equations specifically correlated for each basin or region, which cannot be used for other regions.
- Hydrological reservoir models, such as the hydrological models of the Génie Rural (Rural Engineering) (Perrin *et al.* 2007) with annual time step GR1A, monthly GR2M, daily GR4 J, and hourly GR3H. These are empirical (semi-conceptual) models that assimilate the hydrological behavior of the watershed to cascading

reservoirs, where each one is correlated by an empirical production or routing function, without attempting to integrate flow physics. These models often require, in addition to rainfall data, the integration of certain specific parameters, such as soil moisture status, potential evapotranspiration (PET), etc. Although they sometimes offer better results than those obtained by black box models (Bouanani *et al.* 2013), their limitations are often based on the determination of their specific parameters.

- Hydrological model type ANN (artificial neural network) (Karunanithi *et al.* 1994; Riad *et al.* 2004), such as FA-LM-ANN (Ngo *et al.* 2018), DANN (Banihabib 2016), ANFIS-ICA and ANFIS-FA (Bui *et al.* 2018), etc. Similar to black box type hydrological models, the latter require just as much rainfall and flow data for their calibration. They are built around a stack of interconnected networks of nodes called artificial neurons, where each neuron constitutes in itself a switch (a mathematical function with a result at the output and several variables at the input), whose settings (calibration of the factors of the variables) are pre-established with the help of iterative numerical analyses of the inputs (rainfall) and outputs (flow) of past hydrological events. These models, which are among the most accurate, require a relatively large amount of computing power for their calibrations and are easily deployable for any region having enough data. Since one of their main shortcomings is overlearning (Yamasaki & Ogawa 1993), they can sometimes have difficulty calculating extreme events or events subject to specific conditions that they did not face during their calibrations.

The objective of this study is to develop a conceptual numerical model of FFS under an open source GIS environment, for the north-east study region of Algeria (Seybouse watershed). This model would make it possible at the same time to apprehend the directions of the flows, to localize the floodplains and flood area, calculation of the evolution of flood flows over the entire hydrographic network from rainfall and meteorological data collected in real time, identification of flood risk areas, and the establishment of a georeferenced hydrological database in line with climate change.

To do this, FFS is based on a hydrological simulation model (rainfall-runoff transformation model), specifically developed with the following aims: to be calibrated by taking into account the available data and to overcome some spatial barriers by allowing simulations' calculation on any segment of the hydrographic network, without having to recalibrate all parameters. In contrast to the above-mentioned models, which are built for calculations at localized points in the hydrographic network, the latter require historical data in quantity and quality (rainfall, hydrometric, soil condition parameters, PETs, etc.) for their calibration. The significant lack of these data poses a limitation that is difficult to overcome for the coherent adaptation of the above-mentioned models in this study region. Hence, the choice to move towards the development of a spatialized hydrological model, mainly requiring quality topographic data for its functioning, is largely based on analysis of the hydrographic network, whose segments are assimilated into the main production and routing vectors of the flows.

STUDY AREA

The pilot study zone chosen for the development of this flood forecasting numerical model system is located in the north-east of Algeria, between 35° and 38° north and 06° and 09° east (WGS84), and whose central catchment area is the Seybouse region (Figure 1). This region is characterized by a wide topographical range, stretching from the Saharan Atlas to the Mediterranean Sea via the high plateaus, the Tellian Atlas and the Mediterranean plains, with heights ranging from 0 to 2,328 m. The climate is Mediterranean with heavy rainfalls in winter and hot summers. Rainfall can reach 1,600 mm/year in some areas. This region, on the Algerian–Tunisian border, covers 12 Algerian wilaya departments, and three Tunisian ones. Analysis of the digital elevation model (DEM) of the region revealed 756 complete or partial catchment areas (sub-basin) with a cumulative surface area of 58,676.579 km^2, all having elongated shapes with Gravelius coefficients greater than 1.18 (Gravelius 1914; Sassolas-Serrayet *et al.* 2018), as well as 113,359 watercourse segments up to order 8 on the Strahler classification (Strahler 1957), with a cumulative length of 91,992.654 km (Table 1).

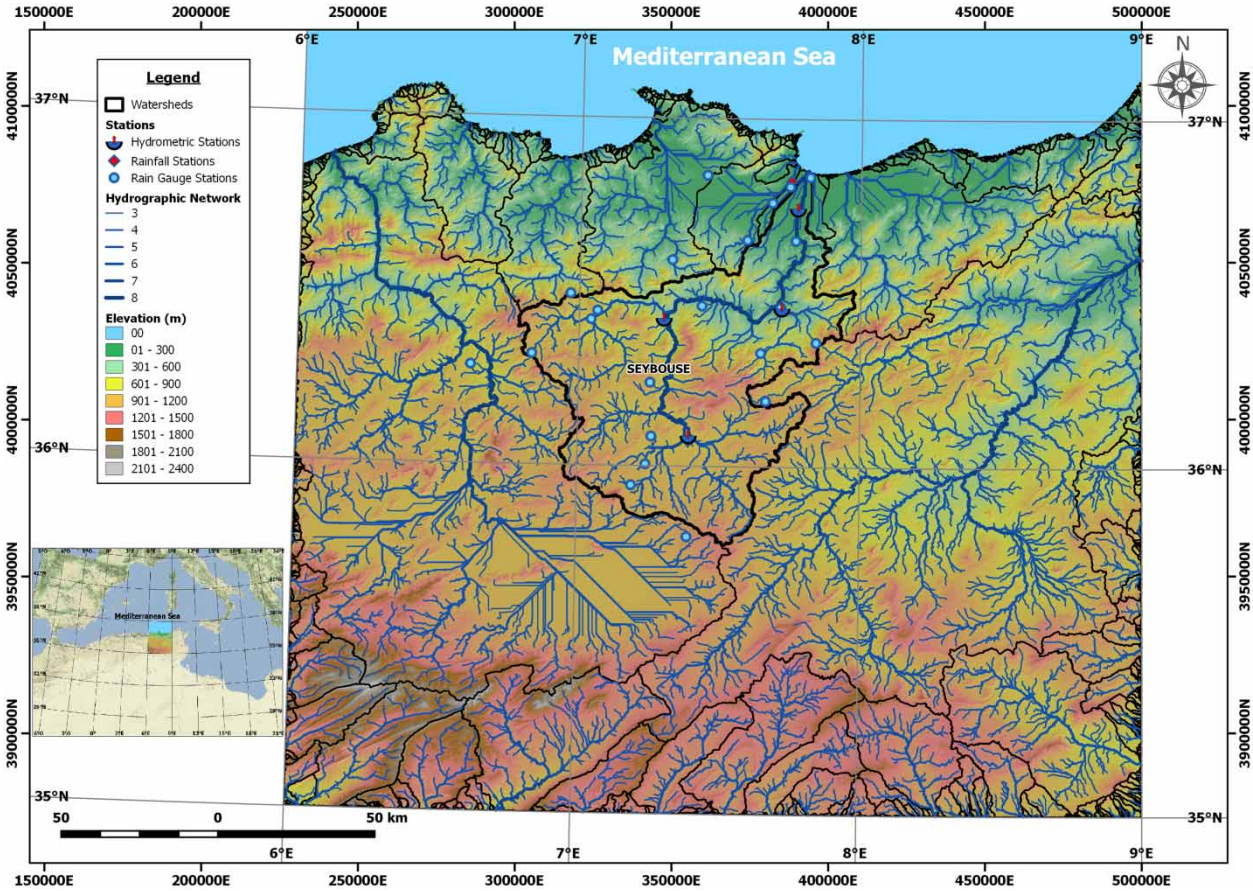

Figure 1 | Location of the study area (WGS84 and UTM-Zone32N).

MATERIALS AND METHODS

Materials used

The materials, data, and parameters used in the development of this numerical flood forecasting model are detailed in Table 2.

Method used

The hydrological model developed in this article for the implementation of this FFS falls into the category of spatialized hydrological models, with a discretization of the watersheds not in raster polygons or other, but rather in watercourse segments of the hydrographic network. Thus, each segment, delimited by confluence nodes of the hydrographic network according to Strahler's classification (Strahler 1957) is considered as a sub-watershed. As a result, it is assigned a close partial area (area drained directly), as well as its own flood conditioning factors, in relation to their neighboring upstream and downstream segments. These factors are mainly estimated through analysis of the various rasters (DEM, slopes, etc.) in the same unit system, in our case the International System (SI), thus making more optimized predictive calculations, since it will be performed from any segment, following the upstream path of the hydrographic network (Figure 2) by using the following simplified principles and formulas.

Assuming that each one of the watercourse segments is in itself a sub-watershed. The latter drain the runoffs from their own surfaces in a period of time (t_R = *internal runoff time of the sub-basins*) and convey the flows from the segments upstream in a second period of time (t_L = *flow travel time*

Table 1 | Characteristics of the main catchment area of the region (Seybouse catchment area) calculated from DEM raster analysis

Parameters	Unit	Values
Area: A	km^2	6,109.106
Perimeter: P	km	733.484
Gravelius compactness index: GC	–	2.647
Length–width of the equivalent rectangle: L_{Rec} – W_{Rec}	km	349.380–17.486
Shape of the catchment area	–	Elongated
Maximum–minimum–average altitude: H_{max} – H_{min} – H_{mean}	m	1,579–00 – 706.19
Altitude at 95% – 50% – 05%: $H_{95\%}$ – $H_{50\%}$ – $H_{05\%}$	m	122.80–806.47 – 1,048.72
Average slope of the watershed: $S_{(Watershed)}$	m/m	0.141
Total length of the hydrographic network	km	9,223.470
Number of segments of the hydrographic network	–	12,290
Drainage density: D_d	km/km^2	1.510
Hydrographic density: D_h	km^{-2}	2.012
Length of the main watercourse: $L_{(Main\_watercourse)}$	km	233.558
Maximum – minimum rating of the main watercourse	m	1,121.78–00
Average slope of the main watercourse: $S_{(Main\_watercourse)}$	m/m	0.0048

along the channels 'Lag time') with ($t_L \subset t_R$). Thus, the flow generated at the outlet of any segment of the watercourse network in response to a given rainfall event is equivalent to the flow generated by the watershed having the same outlet and subjected to the same rainfall event, that is to say equal to the sum of the runoff flows, that flow from the upstream segments to the outlet one, with phase shifts proportional to the distances separating them and the flow velocities.

If we ignore the influence of runoff times on the participative flows' evolution of each segment, or even the flow times along the canals on the evolution of flood flows linked to the phase shift of the participative flows, the theoretical flows and volumes run off within each sub-basin (segment) or watershed can be simplified by Equations (1) and (2):

$$Q_{max(th)} = k_u \cdot C \cdot i \cdot A \tag{1}$$

$$V_{R(th)} = \int_0^{t_d} Q_{max(th)} \cdot dt = Q_{max(th)} \cdot t_d = k_u \cdot C \cdot i \cdot A \cdot t_d \tag{2}$$

With:

$Q_{max(th)}$ the theoretical maximum flow discharge in (m^3/s);

k_u unit conversion factor $\left[k_u = \frac{1}{1000 \cdot 3600}\right]$ for the following units ($m^3/s \leftarrow mm/h$, m^2, s);

C weighted runoff coefficient ($C \approx 0$ *à* 1) representing the overall ratio of the runoff fraction to the total precipitation averaged over the basin;

i average rainfall intensity within the basin in (mm/h);

A basin area in (m^2);

$V_{R(th)}$ the theoretical volume of runoff in (m^3);

t_d the average duration of precipitation within the basin in (s).

By taking Equation (1) and integrating the time factors, which have a considerable influence on the evolution of flood and recession flows within each sub-basin (stream segment), the sum of which, as a function of phase shifts, forms the flood hydrograph at the outlet of the catchment area, we obtain for each sub-basin or segment one of the following three curves (hydrological response) as a function of times (t_R *: internal runoff time of the sub-basins*), (t_L *: flow travel time along the channels 'Lag time'*) and (t_d *: duration of the rainfall event*) (see Figures 3 and 4 and Table 3). The equations of these curves are developed according to the method established by Sokolovsky around 1950 (Sokolovsky 1949, 1959; Khouloud *et al.* 2015), which considers the evolution of flood flows through two parabolic equations, one for the rise of the flood (Equation (3)) and the other for the decline (Equation (4)).

Flow equation as a function of time for increase of the flood

$$Q_{up}(t) = Q_{\max(\text{th})} \left(\frac{t}{t_R}\right)^x \tag{3}$$

Flow equation as a function of time for decrease of the flood

$$Q_{down}(t) = Q_{\max} \left[\frac{\delta t_R - t}{\delta t_R}\right]^y \tag{4}$$

Table 2 | Description of the material and data used

Requirements	Parameters	Uses and applications	Sources
Topographic raster data (35 to 38N; 06 to 09E)	Digital elevation model 1″ arc 30 m at the equator DEM30 (ASTER GDEM 2 -October 2011)	Used for the delimitation of the hydrographic network, the watersheds and some of their characteristics, after analysis via SAGA-GIS	United States Geological Survey (https://earthexplorer.usgs.gov); ASTER GDEM is a product of METI and NASA
Vector land use data (35 to 38N; 06 to 09E)	Strategic infrastructure, roads, bridges, schools, hospitals, etc. (2019)	Used to assess vulnerability and exposure to flood risk	Open Street Map (https://www.openstreetmap.org)
Rain gauge, rainfall and hydrometric data (Seybouse watershed)	7 rain gauge stations, 2 rainfall stations and 4 hydrometric stations (August 1914–February 2014)	Used to calibrate the flood forecast model (simulation of past events using rainfall/rain gauge data and comparison of results with hydrometric data)	Agence Nationale des Ressources en Eau d'Algérie (ANRH) (Algerian National Water Resources Agency)
GIS software	QGIS 3.xxx (GNU General Public License)	Cross-platform GIS software used for the administration, management and display of geographic databases	Quantum GIS (https://www.qgis.org)
GIS analysis software	SAGA GIS 7.xx (Free GPL license)	Cross-platform GIS software used for raster data analysis (DEM)	System for Automated Geoscientific Analyses (http://www.saga-gis.org)
Programming language	Python 3.6.xx With libraries: Numpy; Matplotlib; Openpyxl; PyAutoGUI (Open source license)	Interpreted object programming language, multi-paradigm and multiplatform used for database processing, flood hydrograph prediction calculations and displays (simulations part)	Python (https://www.python.org), Python Libraries (https://pypi.org)
A spreadsheet and SQLite database manager	LibreOffice (Free MPL license), DB Browser for SQLite (Open source license)	For reading, manipulating and saving data in Excel and SQLite – 3 format that can be read and modified under QGIS and Python	LibreOffice (https://www.libreoffice.org), DB Browser for SQLite (https://sqlitebrowser.org)

With a curves power of $[x = 2; y = 3]$, a shape coefficient (δ) depending on the time (t_R) and (t_d) according to Table 3 and a recession time equal to (δt_R).

Between these two periods of flood increase and decrease, expressed by the two parabolic Equations (3) and (4), there may be an intermediate period when the flow stabilizes by aligning with the theoretical maximum flow ($Q_{max(th)}$) in cases where ($t_d > t_R$) (Equation (5)).

Equation of the intermediate peak flow rate in cases where ($t_d > t_R$)

$$Q_{peak}(t) = Q_{\max} = Q_{\max(th)} \tag{5}$$

We thus obtain the following typical hydrological curves or responses, summarized in Figure 4 and Table 3.

Thus, in the three cases, we obtain a total runoff volume (V_R) for each segment, equal to the theoretical runoff volume ($V_{R(th)}$) according to Equations (6)–(12) in accordance with the principle of mass conservation (continuity equation).

As a result, the flood hydrograph obtained at the level of a given segment, in response to any rainfall event, is the product of the curves (hydrological response) of all the segments that constitute its upstream hydrographic network, with phase shifts or latency times proportional to the flow times along the channels (t_L *'Lag time'*) see (Figure 5).

The development of this FFS was based on the stated model in four distinct steps:

1. Creating geo-referenced databases (mainly vectorial in Shapefile and SQLite), whose main core was developed

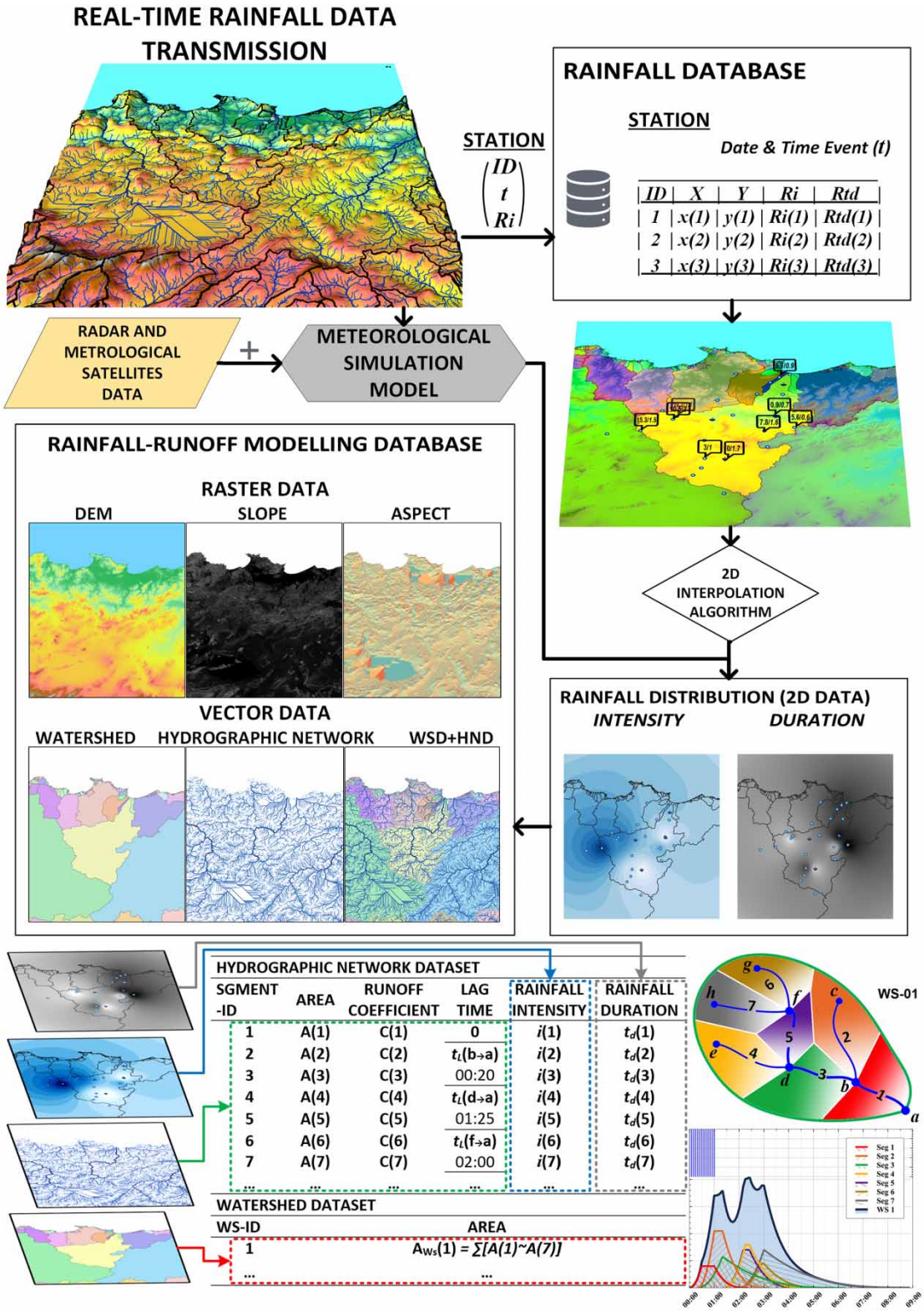

Figure 2 | Summary of FFS and rainfall-runoff model operations.

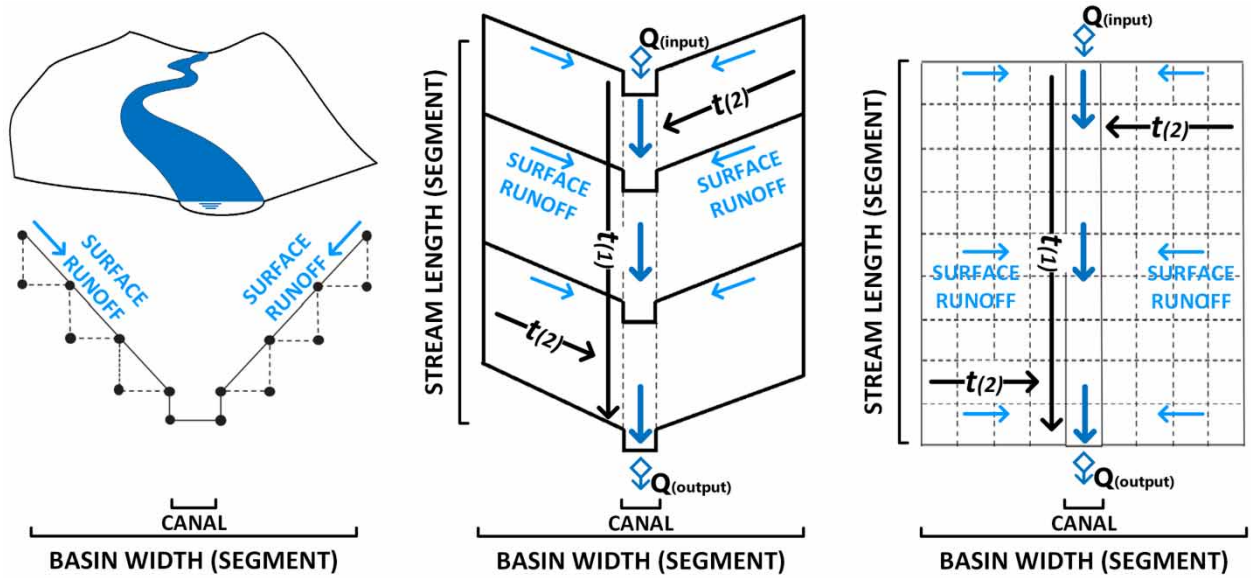

Figure 3 | Representation of river segments of the hydrographic network in sub-basins, with flow times in the canals (lag time) and internal runoff times of the sub-basins $[(t_L = t_{(1)}) \subset (t_R = t_{(1)} + t_{(2)})]$.

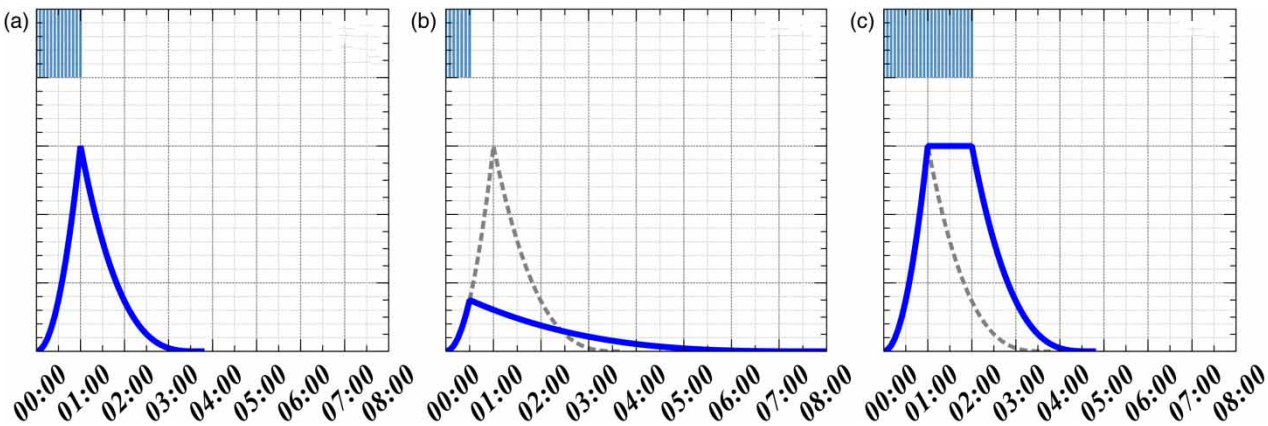

Figure 4 | Representation of the typical curves of the flow discharges produced by each segment (hydrological response) as a function of times (t_d), rainfall duration, and (t_R) runoff time: {(*a*) $t_d = t_R = (t_L + t_{(2)})$ e.g. $t_d = t_R = 1{:}00$}; {(*b*) $t_d < t_R = (t_L + t_{(2)})$ e.g. $t_d = 0{:}30 < t_R = 1{:}00$}; {(*c*) $t_d > t_R = (t_L + t_{(2)})$ e.g. $t_d = 2{:}00 > t_R = 1{:}00$}.

from the analysis of the DEM of the region (Table 2) via the SAGA-GIS software 'notably the Fill Sinks XXL (Wang & Liu) and Basic Terrain Analysis modules'.

2. Writing analysis and enrichment codes for vector databases (in Python 3.6) from the datasets obtained by the DEM analysis.
3. Writing codes that are used for predictive calculations of simulations (in Python 3.6) according to the formulas stated above.
4. Calibrating the model by adapting the codes, physical and hydrological characteristics introduced into the databases.

We can also add a fifth step concerning the exploitation of the model and its correction in the long term – as a dynamic model easily updated.

The parameters composing the equations previously seen, namely: the area (A), the runoff coefficient (C), the

Table 3 | Equations of the flow discharges produced by each segment (hydrological response) as a function of times (t_d) rainfall duration, and (t_R) runoff time

Case (a): $t_d = t_R = (t_L + t_{(2)})$ and Case (b): $t_d < t_R = (t_L + t_{(2)})$	**Case (c): $t_d > t_R = (t_L + t_{(2)})$**	
Case (a) and (b): $t_d \leq t_R$, 2-stroke curve (increasing => decreasing)	Case (c): $t_d > t_R$, 3-stroke curve (increasing => stable => decreasing)	
$Q_{max} = Q_{up}(t_d) = Q_{\max(th)}\left(\frac{t_d}{t_R}\right)^2 \leq Q_{\max(th)}$	$Q_{max} = Q_{up}(t_R) = Q_{max(th)}$	(6a, 6b)
$\delta = \frac{12t_R^2 - 4t_d^2}{3t_R t_d} \geq \frac{8}{3}$	$\delta = \frac{8}{3}$	(7a, 7b)
$V_R = V_{R(up)} + V_{R(down)}$	$V_R = V_{R(up)} + V_{R(peak)} + V_{R(down)}$	(8a, 8b)
$V_{R(up)} = \int_0^{t_d} Q_{up}(t) \cdot dt = Q_{max(th)} \cdot \frac{t_d^3}{3t_R^2}$	$V_{R(up)} = \int_0^{t_R} Q_{up}(t) \cdot dt = Q_{max(th)} \cdot \frac{t_R}{3}$	(9a, 9b)
/	$V_{R(peak)} = \int_0^{t_d - t_R} Q_{peak}(t) \cdot dt = Q_{\max(th)} \cdot (t_d - t_R)$	(10)
$V_{R(down)} = \int_0^{\delta t_R} Q_{down}(t) \cdot dt = Q_{max} \cdot \frac{\delta t_R}{4} = Q_{\max(th)} \cdot t_d \cdot \left(1 - \frac{t_d^2}{3t_R^2}\right)$	$V_{R(down)} = \int_0^{\delta t_R} Q_{down}(t) \cdot dt = Q_{max(th)} \cdot \frac{2t_R}{3}$	(11a, 11b)
$V_R = Q_{\max(th)} \cdot t_d \cdot \left(\frac{t_d^2}{3t_R^2} + 1 - \frac{t_d^2}{3t_R^2}\right) = Q_{\max(th)} \cdot t_d = V_{R(th)}$	$V_R = Q_{\max(th)} \cdot \left(\frac{t_R}{3} + t_d - t_R + \frac{2t_R}{3}\right) = Q_{\max(th)} \cdot t_d = V_{R(th)}$	(12a, 12b)

runoff and travel times (t_R) and (t_L), can be estimated via algorithms, for each segment (sub-basin), according to the methodology below, in order to enable the predictions of hydrographs of floods resulting from rainfall hazards whose intensity and duration parameters (i) and (t_d) are transmitted in real time.

Calculation of drained areas (A)

The model developed for this FFS considers each segment of the river system (delimited between two upstream/downstream confluence nodes) as a sub-watershed, draining its own surface area (A) and carrying flows from the rivers upstream, so each segment is also considered as the outlet of a watershed composed of the upstream segments connected to it.

Thus, it is necessary to start by calculating the areas directly drained by each segment (A), to arrive at the calculation of the flows passing through each of it, by adding up the runoffs from the areas upstream, in the Strahler order (Strahler 1957) from the highest to the lowest, following the opposite path of the hydrographic network. Knowing that the segments whose Strahler order is equal to one have a watershed area equal to their directly drained area (A), we can thus obtain the entire watershed areas of each segment of watercourse.

For this purpose, two difficulties had to be overcome: the first concerned the estimation of the areas (A) attached to each of the segments, which is hampered by the difficulty of delimiting the parcels whose runoff flows directly toward the canals; the latter can be delimited by the water separation lines and thus linked to the quality of DEM data.

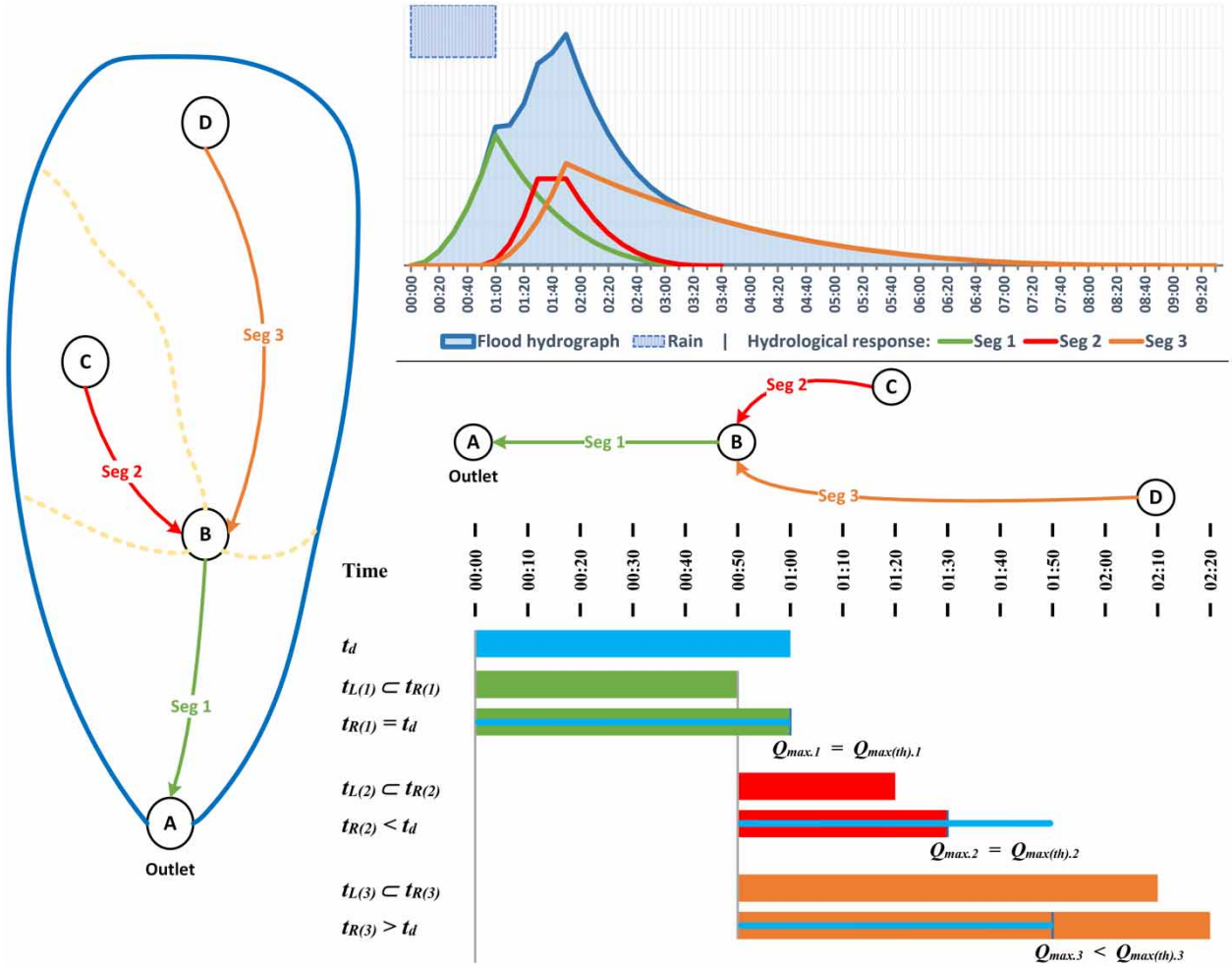

Figure 5 | Illustrative example of the application of the model used for the construction of the flood hydrograph at the outlet of a watershed based on the hydrological responses of the three sub-basins that compose it (three segments that compose its hydrographic network) as well as the flow times along the canals (lag time).

The second concerns the difficulty to rank these segments (sub-basins), namely, which set of sub-basins carry the flow to each segment in order to form with this one a basin of which the last one is an outlet, given the significant number of segments in the study area (113,359 segments).

The analysis of the hydrographic network dataset and its attribute table, generated through the analysis of the region's DEM by the SAGA GIS software, allowed us to solve these two difficulties. In particular, through two important observations, the first is that the hydrographic network of the concerned region is fairly well distributed in space within each of the watersheds and with a Strahler order of up to eight, the second is that despite the absence of segment ordering in the attribute table according to any hydrological reasoning, the latter is rather well provided. It provides us with information on the basin to which each segment belongs, on the Strahler order of the latter, and the system of downstream upstream nodes (A and B) provides us with information on the connections between the segments.

Thus, starting from the observation of the good distribution of the hydrographic network in space, within each catchment area, we were able to estimate approximately the areas directly drained by each segment, based on the assumption that the latter are proportional to the segments' lengths and the surface of the catchment area to which they belong, and this, in line with the principle issued by Horton, which states that the average length of a surface runoff is, in most cases, equal to half of the average distance between channels

of rivers and is therefore approximately equal to the half of the drainage density inverse (Horton 1932, 1945). That is, we have supposed that each linear meter of the hydrographic network within a given watershed drains a partial area equal to the area of the concerned watershed divided by the sum of the lengths of the entire hydrographic network of this one.

Starting from the information provided by the attribute table of the hydrographic network, mainly nodes (A and B) and Strahler orders, we were able to estimate approximately the overall areas drained by each segment, using Python scripts, which allow us to do the hierarchy of the segments (sub-basins), as well as their dynamic mappings on a spreadsheet used for the cumulative travel times (t_L *'Lag time'*).

As an example, we take the case of watershed No. 1 (Figure 6 and Table 4) in our study region.

Where:

- **BASIN_ID and SEGMENT_ID:** Corresponds to the ID of the attribute table of the watershed and segment data (distinctive names)
- **NODE_A and NODE_B:** Corresponds to the number of the start (upstream) and end (downstream) nodes of each segment
- **BASIN:** Corresponds to the number of the watershed (BASIN_ID) to which each segment belongs
- **ORDER:** Corresponds to Strahler's order of each segment, 'Any watercourse without a tributary is assigned an order value equal to one. Similarly, each section

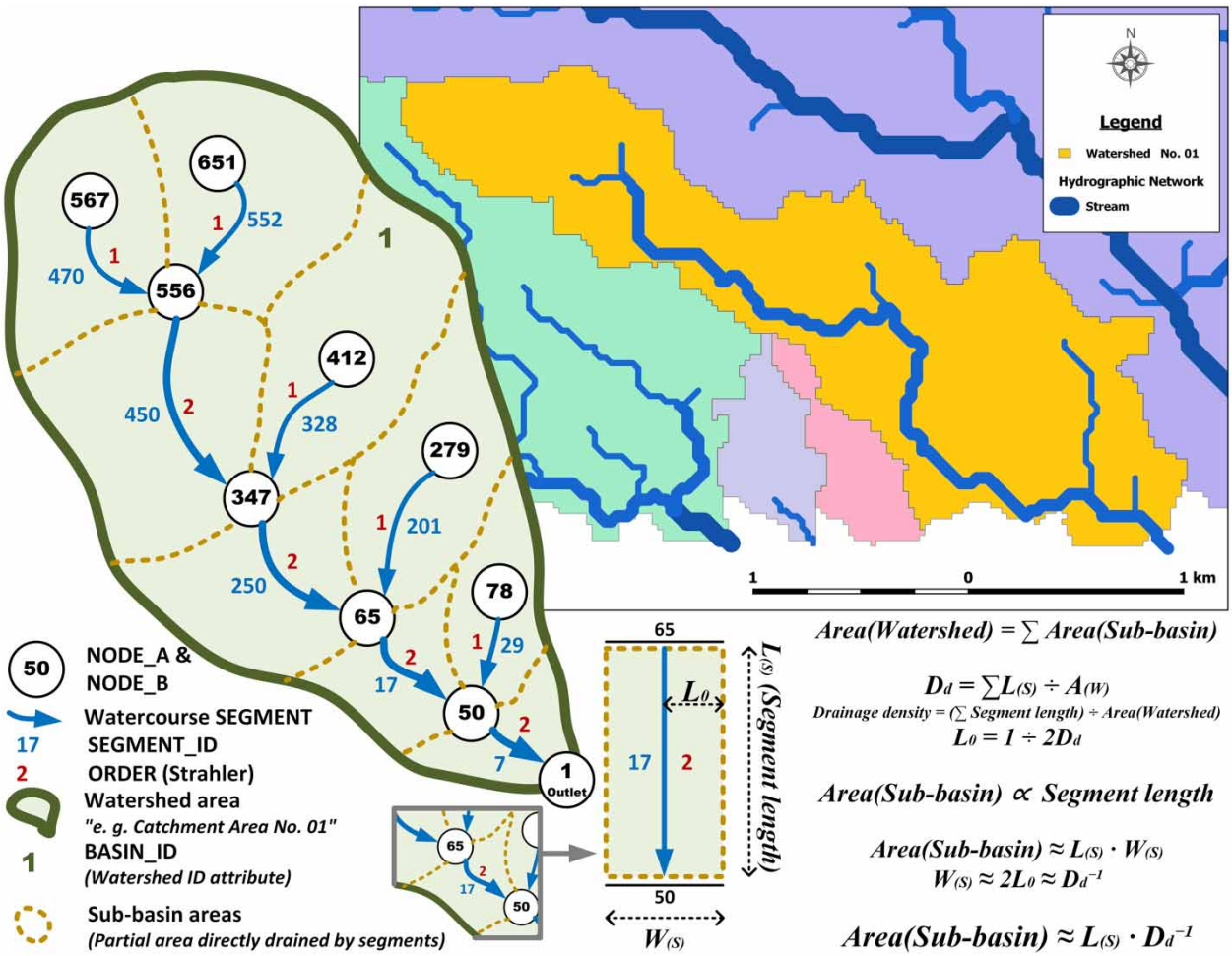

Figure 6 | Discretization of watersheds (example of watershed No. 1).

Table 4 | Example of the estimation of the areas directly drained (*AREA_SEG*) and globally drained (*AREA_SEG_WS*) by each segment within the catchment area No. 1

Table of attributes of the watersheds (e.g., Watershed No. 1)		**Table of attributes of the hydrographic network (e.g., Watershed No. 1)**						**Calculated values**	
BASIN_ID	***AREA_WS***	***SEGMENT_ID***	***NODE_A***	***NODE_B***	***BASIN***	***ORDER***	***LENGTH***	***AREA_SEG***	***AREA_SEG_WS***
1	2,915,555.955	470	567	556	1	1	321.0508508	160,926.1819	160,926.1819
…	…	552	651	556	1	1	223.9398498	112,249.4611	112,249.4611
…	…	201	279	65	1	1	830.1689358	416,120.7385	416,120.7385
…	…	29	78	50	1	1	188.0672342	94,268.37479	94,268.37479
…	…	250	347	65	1	2	1,801.278946	902,887.946	2,164,868.305
…	…	17	65	50	1	2	274.6713893	137,678.5573	2,718,667.601
…	…	328	412	347	1	1	244.9535415	122,782.5376	122,782.5376
…	…	450	556	347	1	2	1,727.731025	866,022.1782	1,139,197.821
…	…	7	50	1	1	2	204.7288478	102,619.9797	2,915,555.955
…	…	…	…	…	…	…	…	…	…
WS	$A_{(WS)}$	*SEG*			*WS*		$L_{(SEG)}$ $\sum L_{(SEG)} = 5{,}816.59$	$A_{(SEG)}$	$A_{(SEG\_WS)}$

resulting from the confluence of two other orders (n) and ($n+1$)'

- **LENGTH:** Corresponds to the length of each stream segment
- **AREA_WS:** Corresponds to the area in (m^2) of each watershed (Field calculated on QGIS)
- **AREA_SEG:** Corresponds to the area in (m^2) directly drained by each stream segment, estimated approximately via Equations (13) and (14):

$$A_{(SEG)\leftarrow(WS=i\,;\,SEG=j)} = \frac{A_{(WS)\leftarrow(WS=i)}}{\sum L_{(SEG)\leftarrow(WS=i)}} \cdot L_{(SEG)\leftarrow(SEG=j)} = D_d^{-1} \cdot L_{(SEG)\leftarrow(SEG=j)} \quad (13)$$

$$\text{With}\left(D_d = \frac{\sum L}{A}\right) \text{equal to the drainage density of the catchment area;} \quad (14)$$

- **AREA_SEG_WS:** Corresponds to the total area drained by each river segment in m^2, estimated approximately by successive additions of ($A_{(SEG)}$) following the hierarchy of segments, established by a Python script working via the information (NODE, BASIN, ORDER) of each segment.

Estimation of runoff coefficients (C)

The runoff coefficient (C) is the ratio between the quantity of water runoff and the quantity of water precipitated at the outlet of the surface considered. It depends on the physical characteristics of the surface: its porosity, permeability, slope, etc., but also on its moisture content (degree of saturation) and green cover. It is thus within this same surface dynamic so not static, it can vary in time, even during the same rainfall event; however, and for practical reasons, the literature in the hydrological field tends, as in this model, to assign it a fixed value in order to simplify the calculations of rainfall-runoff transformations as much as possible.

In the case of this study, the runoff coefficients were weighted for each catchment area ($C_{(WS)}$), but also for each segment ($C_{(SEG)}$), according to several criteria, namely, the nature of the soils, the areas and shapes of the basins or sub-basins (assimilated to the segments), their average slopes, the rainfall intensities, and the green cover.

Each segment was assigned an instantaneous runoff coefficient weighted value, Equation (15), equal to the product of factors resulting from the above-mentioned criteria. The values of these factors, summarized in Table A1 (Annex 1) can be easily modified according to seasonal

changes or special evolution that may be included:

$$C = C_{NS} \cdot C_{A\&GC} \cdot C_{AS} \cdot C_{ARI} \cdot C_{VC} \quad (15)$$

For a precipitation intensity ($i \leq 15\ mm/h$) preponderant in the study area, we obtained the following results (Figure 7).

Approximation of runoff and lag times (t_R) and (t_L)

There are several formulas used for the calculation of concentration times (t_C) of watersheds, also called response times, however none of them are universally accepted. They are generally chosen according to the parameters for which they have been developed or for which they provide consistent results, which may be the size of the basins, their relief, the predominant climates, and the types of development included (urbanized, bare, wooded, etc.). The difference in results obtained between these formulas for the same river basin can sometimes reach 500% (Grimaldi *et al.* 2012), hence the importance of being well documented before deciding on such a parameter, which remains one of the most difficult to estimate. In our case and according to the characteristics of the study region, we have opted for the following formulas (Table 5) according to their fields of application.

The numerical application of Equations (16)–(19), with the addition of a wetting time ($t_{(2)} = 10\ min$) over the 756 watersheds in the study area (Figure 8), showed us how important is the difference between the concentration times obtained by each formula for each watershed. We also noted a spectral distribution of concentration times as a function of the watersheds' surface areas. Equations developed for small basins (such as Kirpich 1940) tend to

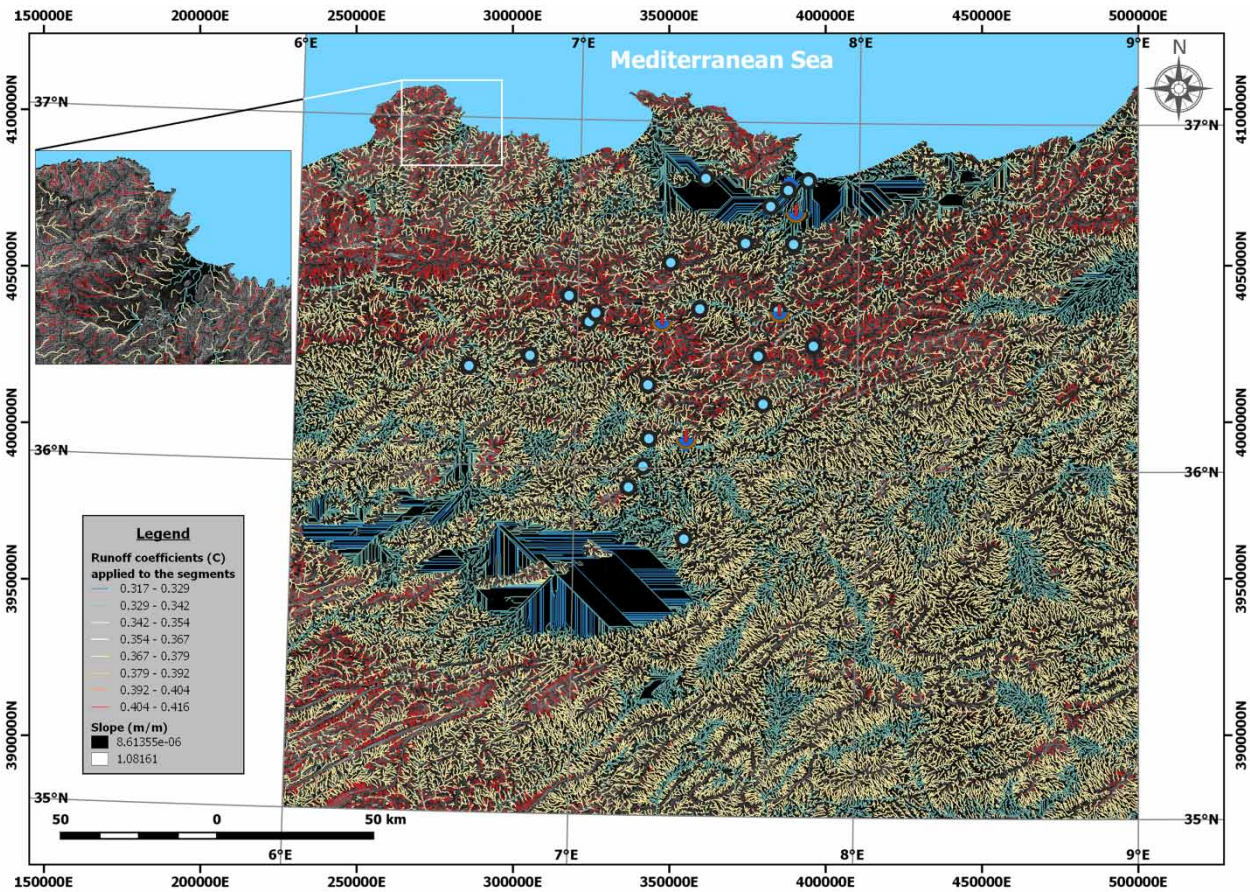

Figure 7 | Runoff coefficients (*C*) applied to sub-basins (segments of the hydrographic network) for preponderant precipitation intensities ($i \leq 15\ mm/h$).

Table 5 | Equations used to estimate watershed concentration times in the study area

Name	Scope of application	Equation
Kirpich (1940)	$0.4 \cdot 10^4 \leq A \leq 81 \cdot 10^4 \quad (m^2)\ 0.03 \leq S \leq 0.12 \quad \left(\frac{m}{m}\right)$	$t_C = 1.1683 \cdot \frac{L^{0.77}}{S^{0.385}}$ (16)
Pasini (1914)	/	$t_C = 0.3888 \cdot \frac{\sqrt[3]{A \cdot L}}{\sqrt{S}}$ (17)
Johnstone & Cross (1949)	$64 \cdot 10^6 \leq A \leq 4200 \cdot 10^6 \quad (m^2)$	$t_C = 61.8162 \cdot \sqrt{\frac{L}{S}}$ (18)
Giandotti (1934)	$170 \cdot 10^6 \leq A \leq 70000 \cdot 10^6 \quad (m^2)$	$t_C = 2.25 \cdot \frac{8\sqrt{A} + 3L}{\sqrt{H_{mean} - H_{min}}}$ (19)

With: t_C = concentration time in (s); A = the catchment area in (m^2); L = the length of the main watercourse in (m); S = the average slope of the catchment area in (m/m); H_{mean}, H_{min} = respectively, the average and minimum heights of the catchment area in (m).

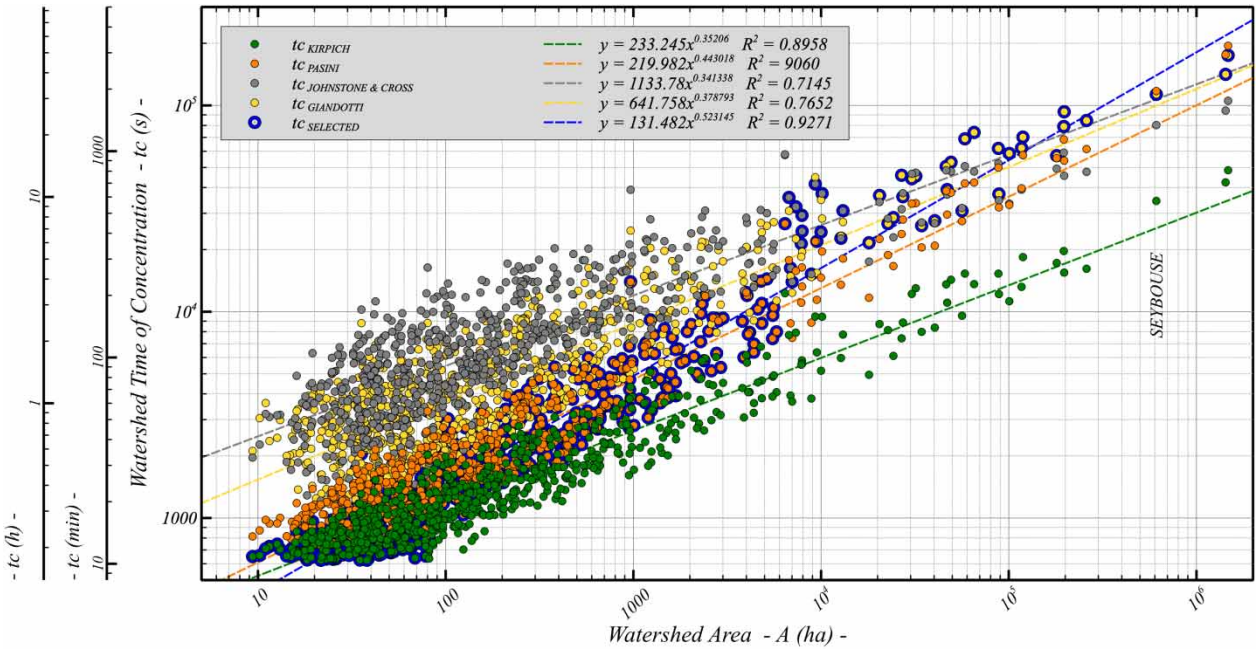

Figure 8 | Distribution of concentration times (t_C) as a function of the watershed areas of the study region, calculated using the Kirpich, Pasini, Johnstone & Cross, and Giandotti equations (on logarithmic scales).

underestimate the concentration times of large basins, and those developed for large basins (such as Johnstone & Cross 1949 and Giandotti 1934) tend to overestimate the concentration times of small basins.

However, these formulas remain inapplicable to the segment scale (according to our discretization) for the simple reason that the various factors of these formulas (basin areas, average lengths and slopes of the main watercourses, etc.) are subjected to rational power exponents, which in this discretization case (if we were to apply them to each segment) their sum cannot be equivalent (e.g., $L = \sum l \rightarrow L^x \neq \sum (l^x)$). It is in this way that we opted for the velocity method, Equation (20), for calculating the average flow times along each segment (t_L *'lag time'*), and the same for an optimal estimation, we compared the results obtained, namely, the sum of the average flow times along

the segments composing the main watercourses of each of the watersheds, with the concentration times of the latter, obtained by the previous conventional formulas (Table 5 and Figure 8).

$$t_L = \frac{L}{v_{mean}} \tag{20}$$

With: $t_L = t_{(1)}$ (Figure 3) = the travel time of the water flow in each segment 'lag time' in (s); L = the length of the segment in (m); v_{mean} = the average flow velocity along each segment in (m/s).

Since the lengths of the river segments remain known, the travel times (lag time) of the latter are therefore linked to the appreciation of the average flow velocities along the channels (segments). These velocities, which generally vary over time as a function of water supply and space as a function of the variability of cross-sectional areas and slopes of rivers, can only be accurately calculated through hydrodynamic flow simulation models known as mechanistic models, such as those based on the Barré de Saint-Venant equations (Barré de Saint-Venant 1871; Saleh *et al.* 2013), which are based on physical principles describing non-permanent, one-dimensional, free surface flows. These models are used for the study of the real movements of a fluid flowing along variable sections, require DEMs with better resolution, and a relatively large capacity of computation for the numerical equations' resolution.

Therefore, due to the difficulty of obtaining such a DEM for large areas and in a desire to simplify the model and optimize calculations, we will consider the flow within each watercourse segment as a uniform and permanent flow, the geometric characteristics are constant along the path of the flow segment: the slope will therefore be considered fixed and equal to the average slope of the concerned segment and the cross section will be considered constant along the segment with variability from one segment to another related to its classification according to the Strahler order. This will result in average flow velocities that vary only from one segment to another, which can be calculated using the Manning–Strickler Equations (21) and (22).

$$v_{mean} = \frac{k_u}{n} \cdot R_h^{2/3} \cdot S^{1/2} = k_s \cdot R_h^{2/3} \cdot S^{1/2} \tag{21}$$

$$R_h = \frac{A_f}{P_f} \tag{22}$$

With: v_{mean} = the average flow velocity in (m/s); n = the Gauckler–Manning coefficient in ($s/m^{1/3}$); k_u = the unit conversion factor ($k_u = 1$ for SI units); k_s = the Strickler coefficient in ($m^{1/3}/s$); R_h = hydraulic radius in (m); S = slope of the hydraulic line or linear hydraulic pressure drop ($S = dh/L$) identical to the slope of the channel bed when the water depths are constant in (m/m), e.g., in case of permanent uniform flow; A_f = the area of the wetted section in (m^2); P_f = the length of the wetted perimeter in (m).

Thus, the approximate estimate of the average flow velocities of each segment therefore depends on: of the average slopes of the rivers extracted from the DEMs, the average values of the Strickler coefficients depending on the properties of the roughness of the river beds, averaged in the case of this study to ($k_s = 30\ m^{1/3}/s$) 'Rivers with meandering and vegetation/rectilinear rivers' and finally, at the cross-sections of the flow (wet sections) assimilated in our case to parabolas Equations (23) and (24) whose mean dimensions (B = flow top width and h = water depth) are proportional to the Strahler orders of the segments according to the Equations (25) and (26) segments developed analytically for the hydrographic network of the study region (Figure A1, Annex 2) and this, by successive approximation of the flow times in the main rivers in relation to the concentration time of the watersheds to which they belong.

$$A_f = \frac{2}{3} Bh \tag{23}$$

$$P_f = B + \frac{8}{3}\frac{h^2}{B} \tag{24}$$

$$B = 1.8 \cdot (O_{Str} + 1) \cdot (log_{10}(O_{Str} + 1)) \tag{25}$$

$$h = 0.4 \cdot (O_{Str} + 1) \cdot (log_{10}(O_{Str} + 1)) \tag{26}$$

With: B = flow top width in (m); h = water depth in (m); O_{Str} = Strahler order of the segment; A_f = the area of the wetted section in (m^2); P_f = the length of the wetted perimeter in (m).

The numerical application of Equations (23)–(26) on Equations (22), (21), and (20) generates Equations (27)–(29), used to estimate the average flow velocities along the channels (segments), as well as the hydraulic travel times of each of them, visible in Figures 9 and 10,

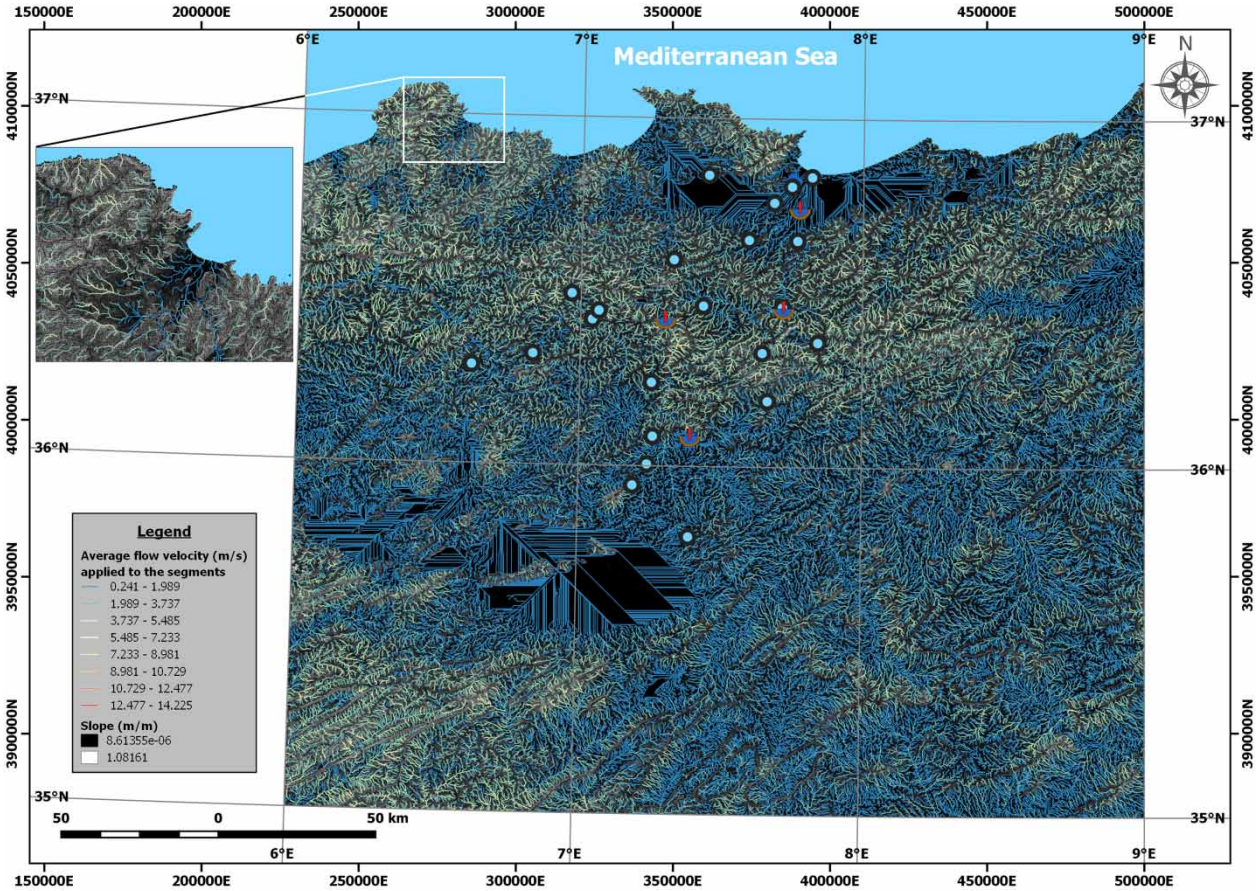

Figure 9 | Average flow velocities along the canals (segments of the hydrographic network).

representing the spatial distribution of the flow rates per segment, and an isochronous representation of the segments according to the flow times to the outlet of the watersheds.

$$R_h = \frac{2B^2h}{3B^2 + 8h^2} = \frac{324 \cdot (O_{Str} + 1) \cdot (log_{10}(O_{Str} + 1))}{1.375 \cdot 10^3} \quad (27)$$

$$v_{mean} = k_s \cdot S^{1/2} \cdot \left(\frac{324 \cdot (O_{Str} + 1) \cdot (log_{10}(O_{Str} + 1))}{1.375 \cdot 10^3}\right)^{\frac{2}{3}} \quad (28)$$

$$t_L = \frac{L}{k_s \cdot S^{1/2} \cdot \left(\frac{324 \cdot (O_{Str} + 1) \cdot (log_{10}(O_{Str} + 1))}{1.375 \cdot 10^3}\right)^{\frac{2}{3}}} \quad (29)$$

With: The assumed uniform permanent flow per segment; R_h = hydraulic radius in (m); B = flow top width in (m); h = water depth in (m); O_{Str} = Strahler order of the segment; v_{mean} = the average flow velocity per segment in (m/s); k_s = the Strickler coefficient in $(m^{1/3}/s)$; S = the slope of the hydraulic line or the linear hydraulic pressure drop $(S = dh/L)$ taken equal to the slope of the channel bed in (m/m).

Rain hazard parameters: intensity (i) and duration (t_d)

These two parameters are supposedly transmitted in real time from the various field stations (rain gauges, radars, etc.) or from weather forecasts directly to the rainfall databases of the Flood Monitoring Center. With the development of ICTs in Algeria in recent years, this should no longer pose a problem for the years to come.

Rainfall hazard data intensity (i) and duration (t_d) will thus be collected in real time, from the various geo-referenced stations or meteorological forecasts, and then interpolated into space according to longitude and latitude

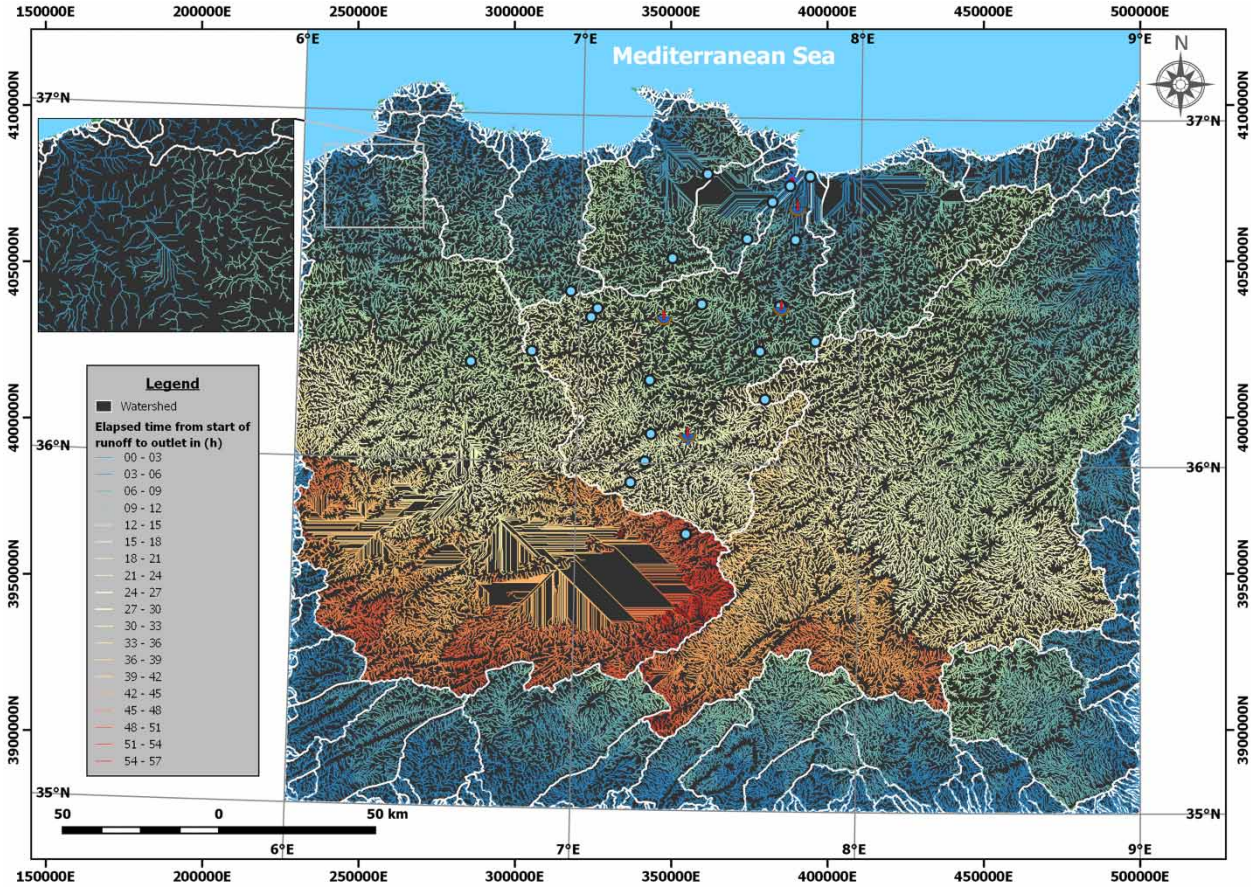

Figure 10 | Average flow times between the start of runoff from each segment of the hydrographic network and the outlets of the watersheds in (*h*) 'isochronous representation of the hydrographic network from the flow times to the outlets'.

via Python scripts in order to obtain the average intensities (i) and durations (t_d) of the weighted rainfall at the level of each segment, in order to enable the launch of predictive calculations.

Model calibration by approximation of parameters (C) and (t_L)

The model is calibrated in two parts: the first part consists of comparing the deviations of the parameters (C) and (t_L) of the segments, with those of the basins to which they belong, in order to get an idea on the concordance of the expected results according to this discretization system (per segment), with those expected by applying classical empirical formulas at the scale of the watersheds.

The comparison of parameter (C), the runoff coefficients, calculated according to Table A1 (Annex 1) for the watersheds and segments, was done as follows: (Equation (30), Figure 11):

$$C_{Watershed(k)} == \frac{1}{A_{Watershed(k)}} \cdot \sum_{i \in [[Watershed_{(k)}]]} C_{Segment(i)} \cdot A_{Segment(i)} \tag{30}$$

With: C = the runoff coefficient (Annex 1); A = the drained area in (m^2).

The average difference obtained between the runoff coefficients of the catchment basins and the weighting of the runoff coefficients of the segments by catchment basin is −0.0186 or −4.496% for all the catchment basins and is +0.015 or +4.248% for the Seybouse catchment basin.

This visible error in the graphs in Figure 11 may be due to the fact that the average slopes of the catchment areas

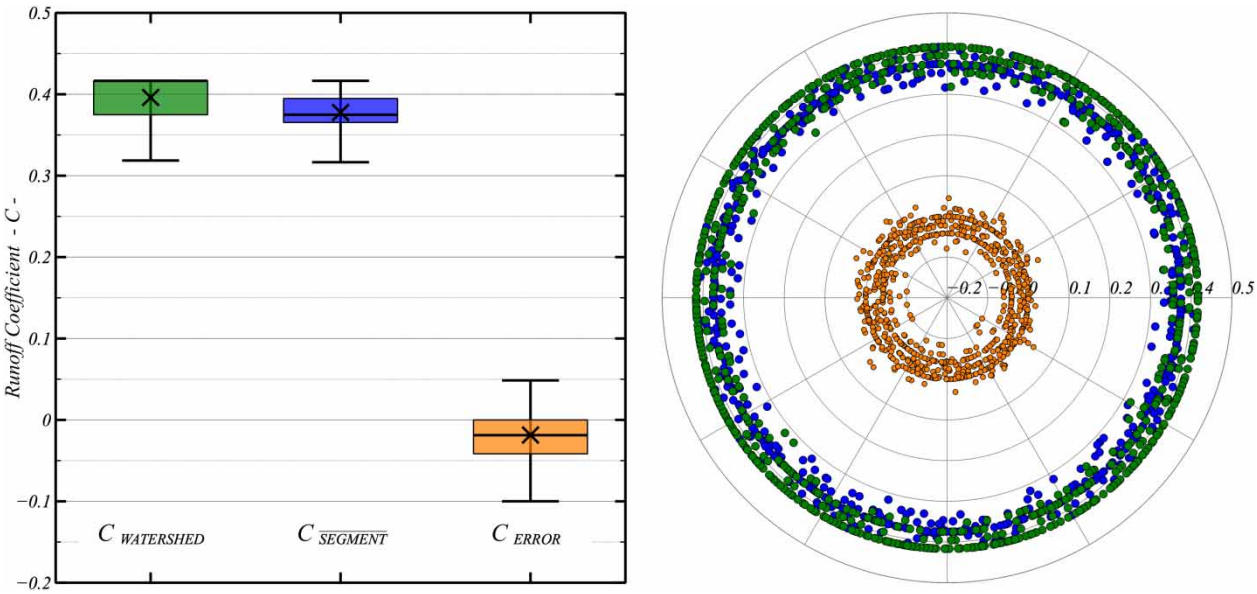

Figure 11 | Comparison of watershed runoff coefficients with segment runoff coefficients' weights by watersheds (Annex 1).

remain greater than the average slopes of the rivers that run through them, and thus, by including the slope factor (S) into the estimation of the runoff coefficient (C), we obtained values slightly lower on the segments than the basins, but this difference can be easily corrected because of the accessibility of the parameters (entered on a SQLite database).

The comparison of the parameter (t_L *'Lag time'*), the travel times along the channels for each segment, calculated according to the velocity equations' method (Equations (20)–(29)), was made with the concentration times of the watersheds calculated according to Table 5, as follows: (Equation (31), Figure 12):

$$t_{C\{Watershed(k)\}} == \sum_{i\in[[Main\_Watercourse\{Watershed_{(k)}\}]]} t_{L\{Segment(i)\}} \tag{31}$$

With: t_C = the watersheds concentration time in (s) (Table 5); t_L = the travel time of the water flow in each segment in (s) Equation (20).

The average of the absolute values of the differences obtained between the travel times of the flows along the main rivers and the concentration times of the catchment basins is 23 min 9 s or 20.74% for all the catchment basins, and is +3 h 33 min 17 s or +11.307% for the Seybouse catchment.

This clear difference in the graphs (Figure 12) is probably due, in part, to the differences between the average slope of the watersheds and that of the main watercourse that flow through them, given the importance of the slope factor (S) in estimating concentration times (t_C) and travel times (t_L *'Lag time'*), although this difference is more difficult to correct but still feasible (using a script written in Python and specifically developed during this study).

The second part of the model calibration must be done as it is used, by comparing the segments' flows of the main river toward the hydrometric stations, with the amplitudes and hourly phase shifts of the rainfall/flow discharge peaks recorded at the rainfall and hydrometric stations, respectively, in order to approximate the parameters (t_L) and (C) as closely as possible.

RESULTS

The reliability of the flood forecasting system developed in this study depends on verifying the performance of its hydrological model. This verification was carried out in two stages. The first consisted of comparing the results of

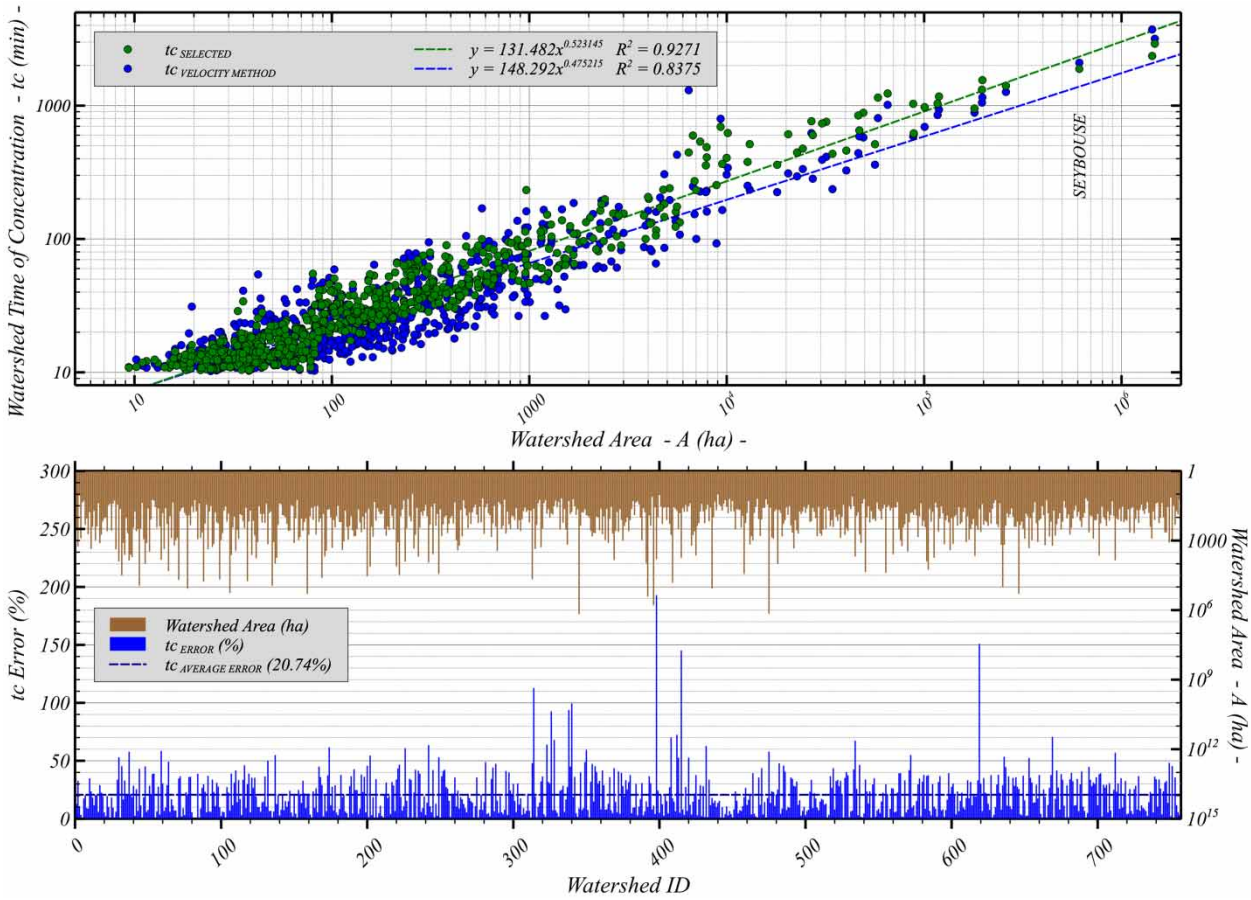

Figure 12 | Comparison of watershed concentration times obtained via the empirical formulas (Table 5 and Figure 8) with the concentration times obtained using the velocity method (flow times along the main watercourses of the watersheds) Equations (20)–(29).

rainfall-runoff transformation simulations of past rainfall events with the hydrometric records of the same dates. The use of historical data from the Seybouse watershed was employed due to the lack, until today, of modern climate infrastructure (with real-time transmission) in the study area. The second step was to compare these results with those obtained by the hydrological simulation tool HEC-HMS, developed by the US Army Corps of Engineers and considered as a standard for hydrological simulations. It has several mathematical models adapted to various environments. In the case of this study, the results were compared with the SCS curve number model for production and the Muskingum model for routing.

Thus, ten simulations were carried out on various rainfall events, which took place between 1974 and 1978 (years when the two dams in the catchment area Oued Charef and Bouhamdane were not yet built) and on two river segments equipped with hydrometric stations, the first one downstream of the catchment area and the second one halfway along its main river. The limited number of these simulated events has been imposed on us, on the one hand, by the fact that they must result from rainfall hazards sufficiently isolated in time to minimize interference and, on the other hand, by the fact of the weak instrumentation over the catchment area whose most of the data available dates from 1973 to 1981. In fact, of the 13 stations in the catchment area for which we have data, four are hydrometric stations (measuring river flows with variable time steps, generally 1 hour), two are rainfall stations (measuring rainfall intensities with variable time steps, generally 30 minutes) and seven are rain gauge stations (measuring rainfall with daily time steps), with an

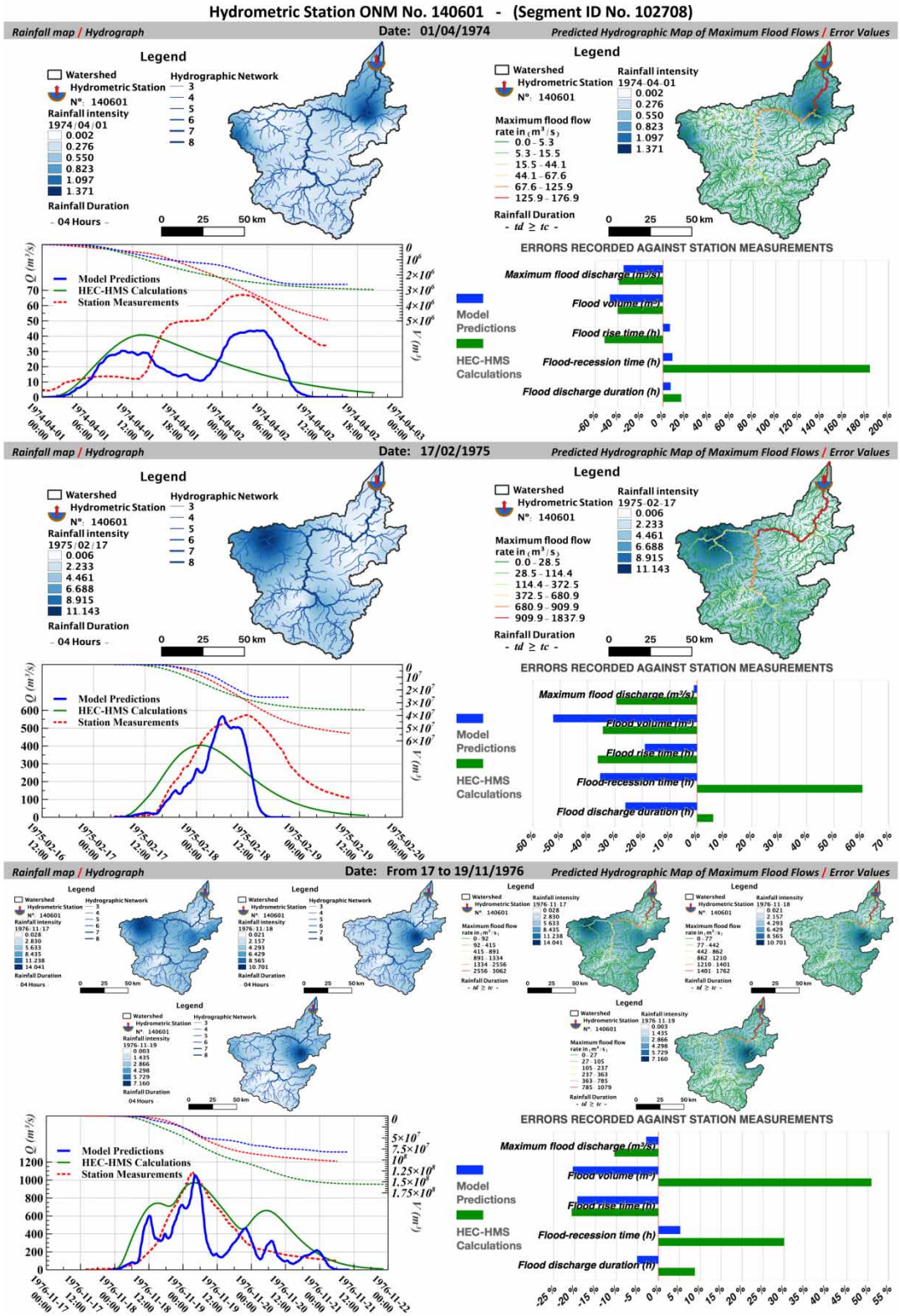

Figure 13 | Comparison of past rainfall hazard simulations results with records from hydrometric station No. 140601 (downstream of the watershed).

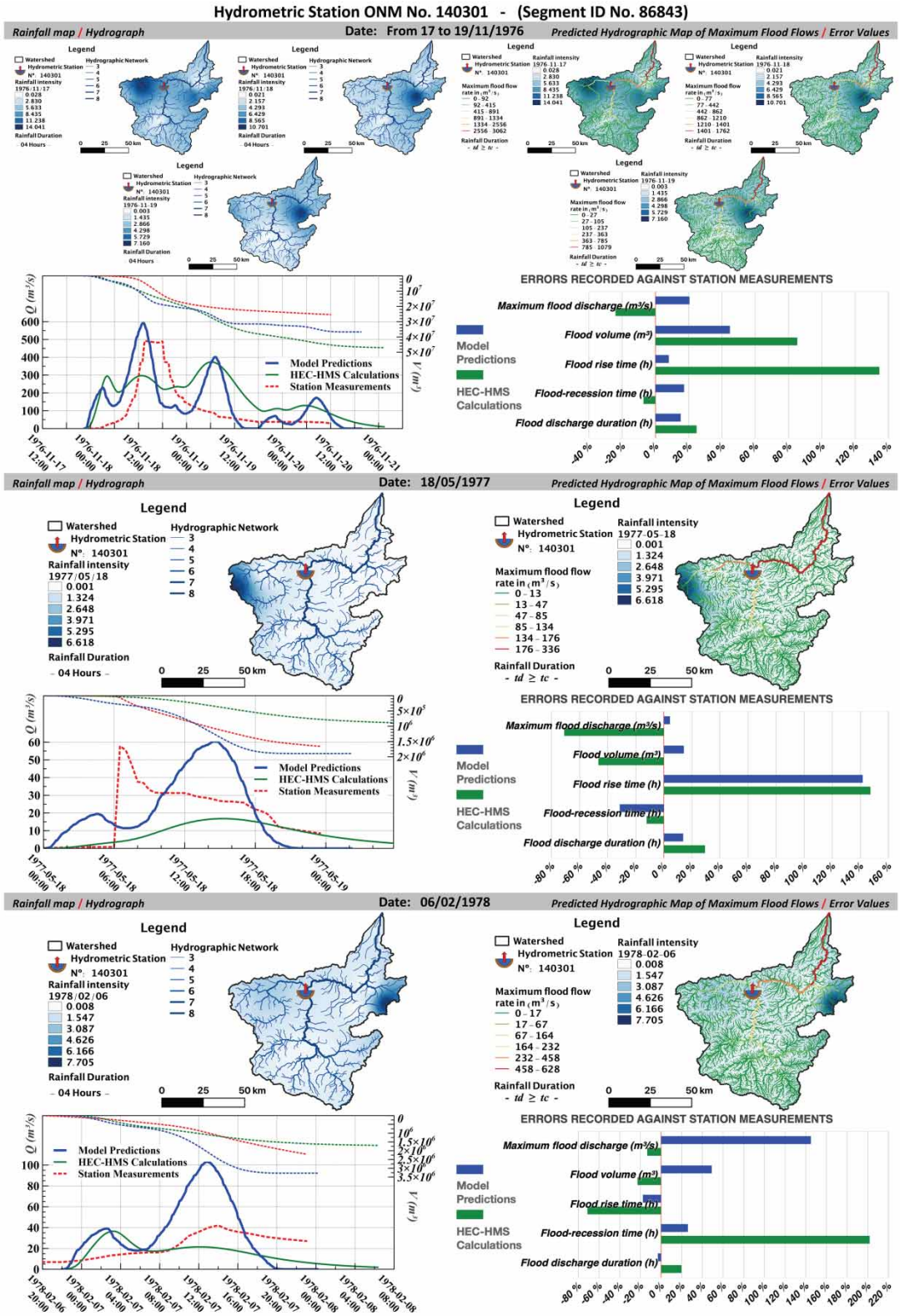

Figure 14 | Comparison of past rainfall hazard simulations results with records from hydrometric station No. 140301 (midway down the main watercourse).

average density of one station per 469.93 km^2, all with alternating and very often unsynchronized periods of operation. In order to provide consistent results, these hydrological models require rainfall data (at narrow time steps, ideally 30 minutes to 2 hours), with a good spatial distribution. In order to avoid distorting the results by introducing erroneous entries, we limited ourselves in this case study to these ten simulations, whose rainfall, rain gauge, and hydrometric data are chronologically intertwined.

The results obtained by the developed model (Figures 13 and 14) gave us mean errors in relation to the hydrometric records of the most relevant parameters, around: 34.8% for the amplitudes of the peak flows' discharge, 38% for the flood volumes, and 11.7% for the base times of surface runoff (Table 6). By way of comparison, the HEC-HMS program gave us error averages for these same parameters, practically of the same order, such as 31.3% for amplitudes of the peak flow discharge, 46.69% for flood volumes, and 17.45% for base times of surface runoff (Table 6).

Comparison of the performance of the model developed in this study with those already proven of the HEC-HMS program (Figure 15) gives us an idea of the relevance of the expected results for future simulations. Thus, the instrumentation of the catchment basins, with modern devices transmitting climate data in real time, would allow, once networked with the simulation calculation unit, to achieve a flood forecasting and management system of the same order of relevance.

In results of the comparison of the models the developed model and the HEC-HMS 'SCS curve number and Muskingum' reference models (Figures 13–15) show a better correlation of the flood flows calculated by the HEC-HMS models with the records of hydrometric station No. 140601 downstream of the catchment area ($R^2 = 0.733$; $NSC = 0.688$) and less for the flood flows of the model developed in this study ($R^2 = 0.651$; $NSC = 0.548$). However, with regard to the most relevant parameters for an FFS, namely, the amplitudes of peak flows, flood volumes and base times of surface runoff, the results obtained by the model developed in this study remain more accurate than those obtained by HEC-HMS. However, the results obtained with the two models used are more consistent for the station downstream of the watershed, compared to the station midway along the main watercourse.

It should also be noted that the commonly used hydrological models, such as HEC-HMS, do not offer the main advantage of the model developed in this study, that is, to know the possibility of instantaneous prediction of flood flow discharges for all segments making up the hydrographic network, thus providing more localized predictions.

Hence, the linking of the climate data collected in real time, with the hydrological model developed in this study,

Table 6 | Average of the errors obtained between the simulation results and the measurements taken by hydrometric stations in the field

Stations	Average of absolute values of errors in % on Station No. 140601 (downstream of the catchment area)		Average of absolute values of errors in % on Station No. 140301 (midway down the main watercourse)		Average of absolute values of errors in % on both stations	
Parameters	**Developed model**	**HEC-HMS**	**Developed model**	**HEC-HMS**	**Developed model**	**HEC-HMS**
Maximum flood flows	13.01% (± 20.70 m^3/s)	26.40% (± 103.27 m^3/s)	56.59% (± 54.67 m^3/s)	36.11% (± 54.87 m^3/s)	34.80% (± 37.69 m^3/s)	31.25% (± 79.07 m^3/s)
Flood volumes	40.02% (± 1.73 · 10^7 m^3)	41.84% (± 2.44 · 10^7 m^3)	36.02% (± 4.22 · 10^6 m^3)	51.54% (± 7.63 · 10^6 m^3)	38.02% (± 1.08 · 10^7 m^3)	46.69% (± 1.60 · 10^7 m^3)
Flood rise time	14.88% (± 4.92 h)	36.29% (± 10.97 h)	55.76% (± 4.25 h)	117.70% (± 13.28 h)	35.32% (± 4.58 h)	76.99% (± 12.13 h)
Flood-recession time	16.33% (± 4.03 h)	91.27% (± 16.67 h)	24.83% (± 5.22 h)	73.76% (± 7.86 h)	20.58% (± 4.63 h)	82.52% (± 12.26 h)
Flood discharge duration	12.71% (± 7.17 h)	10.28% (± 5.69 h)	10.66% (± 4.36 h)	24.61% (± 8.97 h)	11.69% (± 5.76 h)	17.45% (± 7.33 h)

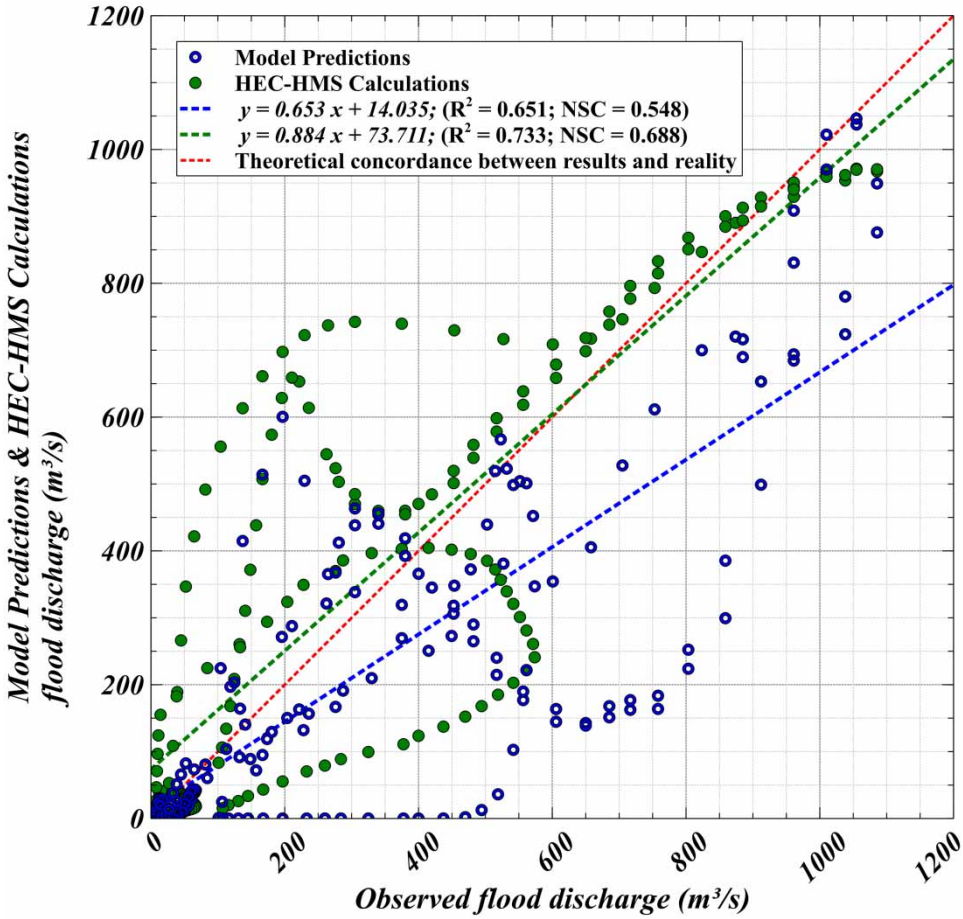

Figure 15 | Comparison of the prediction results established by the developed model and the HEC-HMS simulation tool with the measurements of hydrometric station No. 140601.

would enable the almost instantaneous prediction of flood flows recorded at any segment of the hydrographic network. The automated cross-referencing on GIS of the predicted flows with the known hydraulic capacities of the various streams, bridges, evacuation, protection works, etc. will highlight the supposedly flood-prone segments, with a sufficient time margin for any preventive interventions.

DISCUSSION

Comparison of the model developed in this study with those of the HEC-HMS hydrological program highlights the fact that in both, the accuracies obtained are below those desired, despite the different concepts of the models and the parameters they use. This indicates that the plausible causes of these precision defects probably come from the main variables introduced in both cases, namely, the rainfall hazard variables, whose spatial distribution remained insufficient.

From the ten simulations performed, we obtained accuracies in the order of 65.2% for peak flow amplitudes and 88.3% for surface runoff base times, with trends for the main parameters (peak flows, flood volumes, and base time) slightly downward for the station downstream of the watershed and strongly upward for the station midway along the main watercourse. These trends may be due in part to the influence of certain hydrological phenomena which are not taken into account by this model, which focuses exclusively on surface runoff, such as subsurface (hypodermic) or deep (groundwater) flows, which can significantly influence these parameters, by impacting surface runoff by infiltration and outcropping of precipitated

waters, respectively, upstream and downstream of the watersheds along the depths of aquifers (Ala-aho *et al.* 2017). Among other things, a spatial distribution of flood flow discharges has been observed that is not always in phase with the hydrometric station records. This is probably due to the use of rain gauge station records because of lack of data for which the time steps are insufficient to obtain good precision.

These precisions remain, of course, much more illustrative than descriptive of the model, because the model is nothing more or less than a minimalist calculator of river flows, calculating in predefined time steps the accumulation of surface runoff of the segments of a hydrographic network according to their phase shifts. These accuracies can, therefore, be improved when the various factors conditioning the runoff assigned to each of the segments of concerned network are configured, just as they can be reduced to the point of judging the model to be too simplistic to be descriptive of the complexity of hydrological responses in the watershed. In either case, we would need more qualitative and quantitative measurements of precipitation (rainfall data) and stream flows (hydrometric recording) and more simulations to support our hypotheses.

PROSPECTS FOR DEVELOPMENT AND USE

Although this model provides consistent and fairly realistic results, it is still minimalist and indicates many gaps that could be the subject of future research, including:

- The lack of management of the variability of soil infiltration capacities according to their moisture conditions, which plays an important role in the dynamics of the watershed from one hazard to another (Ruggenthaler *et al.* 2016). This variability was simplified in this model by static runoff coefficients, induced to overestimate the runoff flows on dry land and thus to overestimate the flows and flood volumes generated following dry periods when the soil is more permeable.
- Similarly, the lack of support for the variability of flow velocities as a function of fluctuations in stream flow rates and wet sections, as well as seasonal changes in green cover. Simplified in this model by static flow velocities per segment (velocity method) for estimating response times, sometimes leads to errors in the evaluation of the last one (U.S. Department of Agriculture and Natural Resources Conservation Service 2010). If this problem can be overcome, by incorporating a hydrodynamic flow model using Saint-Venant's equations or others, this would require more data (mainly those of the soils of the hydrographic network: detailed topographies, channel roughness, vegetation, etc.), which would considerably increase the number of parameters and the volume of calculations required for each simulation.
- The lack of management of the hydrological mechanisms responsible for the so-called deep water table flows (Kirchner 2009; Guérin *et al.* 2019) and subsurface flows known as hypodermic flows (Freeze 1972) induce errors that can occur in various ways, such as: excess flow or flows disconnected from rainy hazards or from other watersheds, flowing through aquifers that flow to the surface as is the case for low water flows, or rapid discharges of flows that match rainfall hazards due to the piston effect that can occur under some conditions in subsurface flows.
- The simplification of the areas' calculations drained by each segment according to our discretization of the watersheds into segments (Horton architecture) generates errors that can be more or less important according to the homogeneity of the distribution of the hydrographic network within the same watershed, thus we will have overestimations of these areas in some regions with high hydrographic density and underestimations for those with low hydrographic density. These errors rarely exceed 20% in the case of this study, and can be greatly limited, by first fragmenting the large catchment areas into several basins, of which Strahler's order of the hydrographic network does not exceed six.
- The automation of predictive calculations following the flow through the hydrographic network makes it difficult but not impossible to integrate the mechanisms of flood spreading, which can occur along the water paths, whether due to natural obstacles (topographical depressions, lakes, etc.) or artificial ones (dams, dikes, etc.).
- Finally, it should be noted that this model as it is presented only handles floods due to rain hazards, but there are other types of floods around the world, such as those due to snowmelt caused by rising temperatures, which can be studied differently.

In return for these shortcomings, this model has a number of advantages, which make it a major tool in flood forecasting and management, mainly in emerging countries, low-income watershed agencies, or small communities wishing to protect themselves against floods. Among these advantages are:

- Consistent and realistic predictions that can be improved as usage progresses by customizing the calculation factors.
- Rapid deployment in any watershed.
- A very advantageous deployment and administration cost (almost zero).
- Requiring few human resources for either deployment or day-to-day management.
- Requiring few parameters (intensity and duration of precipitation) and little computing power to operate, all with open source tools that can run on desktop computers under any mainstream OS.
- Fast execution of prediction calculations that can be performed on any segment of the hydrographic network (stable model with almost instantaneous results).
- Simple model, easily accessible and editable at will, whether for parameters or code, allowing the calibration and customization as it is used.

CONCLUSION

Flood events' management is based in part on anticipating and predicting phenomena that may generate floods with or without flooding. A study conducted in the United States in 2002 by the National Hydrologic Warning Council (NHWC 2002) revealed that anticipating these phenomena by even 1 hour, in the case of flash floods generally occurring in small hilly or highly reactive catchment areas, would reduce the damage that could be caused by effective and appropriate intervention by at least 10%. This reduction can reach 35% in the case of slow floods that generally occur in large catchment areas or those with low reactivity, according to the United Nations Office for Disaster Risk Reduction (Pilon 2002).

The completion and deployment of this model at the scale of the Seybouse pilot region (north-east Algeria) required the implementation of three disciplines, which will be increasingly linked: hydrology, geographic information systems, and data sciences. Working together with the aim of approaching a technically complex problem: the forecasting of flood flows on the scale of a hydrographic network, in a procedural manner, first by discretizing the catchment areas into meshes, in the case of this study according to the segments composing their hydrographic network, then by integrating analytically the flow parameters, like the factors of an artificial neural network, to finally predict the flood hydrographs resulting from the sum of the flow discharge contributions of each segment of said hydrographic network.

The deployment of such a flood management and forecasting model would make it possible to anticipate peak flows and flood volumes with very low cost for any segment of the hydrographic network, ranging from a few hours in the case of the use of real-time rainfall data to a few days in the case of the use of weather forecast data, with accuracies that tend to decrease in proportion to the forecast times. This would make it possible, among other things, to monitor and anticipate the flood risk at sensitive points in the hydrographic network (various structures, bridges, urban areas, industrial zones, etc.) and to limit plausible damage as far as possible by adapting a crisis management plan (traffic plan, access road for interventions, evacuation zone, etc.).

This minimalist conceptual model therefore remains one of the possible solutions to be deployed for flood management and forecasting, attractive due to its cost and simplicity. However, it still needs to be further improved, in particular by incorporating mechanisms governing some hydrological phenomena such as subsurface and deep flows or by automating the variability of soil infiltration and runoff capacities according to the moisture conditions.

SUPPLEMENTARY MATERIAL

The Supplementary Material for this paper is available online at https://dx.doi.org/10.2166/wcc.2020.265.

REFERENCES

Agirre, U., Goñi, M., López, J. J. & Gimena, F. N. 2005 Application of a unit hydrograph based on subwatershed division and comparison with Nash's instantaneous unit hydrograph.

Catena **64** (2–3), 321–332. https://doi.org/10.1016/j.catena.2005.08.013.

Ala-aho, P., Soulsby, C., Wang, H. & Tetzlaff, D. 2017 Integrated surface-subsurface model to investigate the role of groundwater in headwater catchment runoff generation: a minimalist approach to parameterisation. *Journal of Hydrology* **547**, 664–677. https://doi.org/10.1016/j.jhydrol.2017.02.023.

Al-Juaidi, A. E. M., Nassar, A. M. & Al-Juaidi, O. E. M. 2018 Evaluation of flood susceptibility mapping using logistic regression and GIS conditioning factors. *Arabian Journal of Geosciences* **11** (24), 765. https://doi.org/10.1007/s12517-018-4095-0.

Banihabib, M. E. 2016 Performance of conceptual and black-box models in flood warning systems. *Cogent Engineering* **3** (1), 1127798. https://doi.org/10.1080/23311916.2015.1127798.

Barré de Saint-Venant, A. J. C. 1871 Théorie du mouvement non permanent des eaux, avec application aux crues des rivières et à l'introduction des marées dans leur lit. (Theory of the non-permanent movement of water with applications to the flooding of rivers and the introduction of tides into their beds). *Comptes Rendus Hebdomadaires des Séances de L'Académie des Sciences* **73** (147), 237–240. https://gallica.bnf.fr/ark:/12148/bpt6k3030d/f237.image.

Beven, K. J. & Kirkby, M. J. 1979 A physically based, variable contributing area model of basin hydrology/Un modèle à base physique de zone d'appel variable de l'hydrologie du bassin versant. *Hydrological Sciences Bulletin* **24** (1), 43–69. https://doi.org/10.1080/02626667909491834.

Bouanani, R., Baba-hamed, K. & Bouanani, A. 2013 Utilisation d'un modèle global pour la modélisation pluie-débit: cas du bassin d'Oued Sikkak (NW algérien). (Use of a global model for rain-flow modeling: case of the Oued Sikkak basin (Algerian NW). *Nature et Technologie* **9**, 61–66. https://www.univ-chlef.dz/Revuenatec/Issue_09_Art_C_06.pdf

Bouvier, C. 1994 *MERCEDES (Maillage Elémentaire Régulier Carré pour l'Etude Des Ecoulements Superficiels) Principes du modèle et notice d'utilisation. (MERCEDES Regular Square Elementary Mesh for the Study of Surface Flows: Principles of the Model and Instructions for use)*. ORSTOM, Montpellier, France.

Bouvier, C., Fuentes, M. G. & Dominguez, M. R. 1994 *MERCEDES: un modèle hydrologique d'analyse et de prévision de crues en milieu hétérogène" in Crues et inondations. (MERCEDES: A Hydrological Model for Analysis and Forecasting of Floodsin Heterogeneous Environments in Floods and Floods)*. SHF, Paris, France, pp. 257–260. http://www.documentation.ird.fr/hor/fdi:41790

Bui, D. T., Panahi, M., Shahabi, H., Singh, V. P., Shirzadi, A., Chapi, K., Khosravi, K., Chen, W., Panahi, S., Li, S. & Ahmad, B. B. 2018 Novel hybrid evolutionary algorithms for spatial prediction of floods. *Scientific Reports* **8** (1), 15364. https://doi.org/10.1038/s41598-018-33755-7.

CEPRI 2017 *Prévision et anticipation des crues et des inondations. (Forecasting and Anticipating Floods and Floods)*. www.cepri.fr

Chow, V. T., Maidment, D. R. & Mays, L. W. 1988 *Applied Hydrology*. McGraw-Hill, New York, USA.

Datin, R. 1999 Développement d'outils opérationnels pour la prévision des crues rapides. Prise en compte de la variabilité spatiale de la pluie dans TOPMODEL. (The development of tools for flash flood forecasting. The introduction of spatial variability in TOPMODEL). *La Houille Blanche* **7–8**, 13–20. https://doi.org/10.1051/lhb/1999076.

Donat, M. G., Lowry, A. L., Alexander, L. V., O'Gorman, P. A. & Maher, N. 2016 More extreme precipitation in the world's dry and wet regions. *Nature Climate Change* **6** (5), 508–513. https://doi.org/10.1038/nclimate2941.

Edson, C. G. 1951 Parameters for relating unit hydrographs to watershed characteristics. *Eos, Transactions American Geophysical Union* **32** (4), 591–596. https://doi.org/10.1029/TR032i004p00591.

ESPADA 2005 *Évaluation et Suivi des Pluies en Agglomération pour Devancer l'Alerte. (ESPADA: an Innovative Tool for Real Time Urban Flood Management)*. ESPADA, Ville de Nîmes, France. http://documents.irevues.inist.fr/bitstream/handle/2042/25386/0793_270raymond.pdf

FEON – Hydrodaten 2007 *Federal Office for the Environment – Hydrological Data and Forecasts Hydrodaten*. FEON – Hydrodaten, Switzerland. https://www.hydrodaten.admin.ch/en/

Freeze, R. A. 1972 Role of subsurface flow in generating surface runoff: 2. Upstream source areas. *Water Resources Research* **8** (5), 1272–1283. https://doi.org/10.1029/WR008i005p01272.

Giandotti, M. 1934 Previsione delle piene e delle magre dei corsi d'acqua. *Istituto Poligrafico dello Stato* **8**, 107–117.

Gravelius, H. 1914 *Flusskunde*. G.J. Göschen, Berlin, Germany. https://books.google.dz/books?id=Zds0AQAAMAAJ

Grimaldi, S., Petroselli, A., Tauro, F. & Porfiri, M. 2012 Time of concentration: a paradox in modern hydrology. *Hydrological Sciences Journal* **57** (2), 217–228. https://doi.org/10.1080/02626667.2011.644244.

Guérin, A., Devauchelle, O., Robert, V., Kitou, T., Dessert, C., Quiquerez, A., Allemand, P. & Lajeunesse, E. 2019 Stream-discharge surges generated by groundwater flow. *Geophysical Research Letters* **46** (13), 7447–7455. https://doi.org/10.1029/2019GL082291.

Habets, F. & Saulnier, G. M. 2001 Subgrid runoff parameterization. *Physics and Chemistry of the Earth, Part B: Hydrology, Oceans and Atmosphere* **26** (5–6), 455–459. https://doi.org/10.1016/S1464-1909(01)00034-X.

Hirabayashi, Y., Mahendran, R., Koirala, S., Konoshima, L., Yamazaki, D., Watanabe, S., Kim, H. & Kanae, S. 2013 Global flood risk under climate change. *Nature Climate Change* **3** (9), 816–821. https://doi.org/10.1038/nclimate1911.

Horton, R. E. 1932 Drainage-basin characteristics. *Eos, Transactions American Geophysical Union* **13** (1), 350–361. https://doi.org/10.1029/TR013i001p00350.

Horton, R. E. 1945 Erosional development of streams and their drainage basins: hydrological approach to quantitative

morphology. *Bulletin of the Geological Society of America* **56** (3), 275–370. https://doi.org/10.1130/0016-7606(1945)56[275:EDOSAT]2.0.CO;2.

IPCC 2007 *Climate Change 2007: Synthesis Report. Contribution of Working Groups I, II and III to the Fourth Assessment Report of the Intergovernmental Panel on Climate Change*. IPCC, Geneva, Switzerland. https://www.ipcc.ch/pdf/assessment-report/ar4/syr/ar4_syr_full_report.pdf

Johnstone, D. & Cross, W. P. 1949 *Elements of applied hydrology*. Ronald Press, New York, USA.

Karunanithi, N., Grenney, W. J., Whitley, D. & Bovee, K. 1994 Neural networks for river flow prediction. *Journal of Computing in Civil Engineering* **8** (2), 201–220. https://doi.org/10.1061/(ASCE)0887-3801(1994)8:2(201).

Khouloud, G., Ahlem, G. & Raouf, M. M. 2015 Proposal of installations to protect watersheds in the lower valley of the Medjerda, Tunisia. *International Research Journal of Earth Sciences* **3** (1), 54–65. http://www.isca.in/EARTH_SCI/Archive/v3/i1/9.ISCA-IRJES-2014-048.pdf

Kirchner, J. W. 2009 Catchments as simple dynamical systems: catchment characterization, rainfall-runoff modeling, and doing hydrology backward. *Water Resources Research* **45** (2), 1–34. https://doi.org/10.1029/2008WR006912.

Kirpich, Z. P. 1940 Time of concentration of small agricultural watersheds. *Civil Eng.* **10** (6), 362.

Kohler, M. A. & Linsley, R. K. 1951 *Predicting the Runoff From Storm Rainfall*, Vol. 30. US Department of Commerce, Weather Bureau, Washington DC, USA, pp. 01–10. https://www.nrc.gov/docs/ML0819/ML081900279.pdf

Ngo, P. T. T., Hoang, N.-D., Pradhan, B., Nguyen, Q. K., Tran, X. T., Nguyen, Q. M., Nguyen, V. N., Samui, P. & Tien Bui, D. 2018 A novel hybrid swarm optimized multilayer neural network for spatial prediction of flash floods in tropical areas using Sentinel-1 SAR imagery and geospatial data. *Sensors* **18** (11), 3704. https://doi.org/10.3390/s18113704.

NHWC 2002 *Use and Benefits of the National Weather Service River and Flood Forecasts*. National Hydrologic Warning Council (May), p. 21.

Pasini, F. 1914 Relazione sul progettodella bonifica renana.

Perrin, C., Michel, C. & Andréassian, V. 2007 *Modèles Hydrologiques du Génie Rural (GR). (Hydrological Models of Rural Engineering)*. http://www.cemagref.fr/webgr

Pilon, P. J. 2002 *Guidelines for Reducing Flood Losses*. Diane Publishing Co, Darby, PA, USA. http://lib.riskreductionafrica.org/bitstream/handle/123456789/1045/3428.Guidelines for Reducing Flood Losses.pdf?sequence=1

Quinn, P. F., Beven, K. J. & Lamb, R. 1995 The in(a/tan/β) index: how to calculate it and how to use it within the topmodel framework. *Hydrological Processes* **9** (2), 161–182. https://doi.org/10.1002/hyp.3360090204.

Riad, S., Mania, J., Bouchaou, L. & Najjar, Y. 2004 Rainfall-runoff model using an artificial neural network approach. *Mathematical and Computer Modelling* **40** (7–8), 839–846. https://doi.org/10.1016/j.mcm.2004.10.012.

Riggs, H. C. 1985 *Streamflow Characteristics (Vol. 22)*. Developments in Water Science, Elsevier, Amsterdam, The Netherlands. https://www.sciencedirect.com/bookseries/developments-in-water-science/vol/22

Rodríguez-Iturbe, I. & Valdés, J. B. 1979 The geomorphologic structure of hydrologic response. *Water Resources Research* **15** (6), 1409–1420. https://doi.org/10.1029/WR015i006p01409.

Ruggenthaler, R., Meißl, G., Geitner, C., Leitinger, G., Endstrasser, N. & Schöberl, F. 2016 Investigating the impact of initial soil moisture conditions on total infiltration by using an adapted double-ring infiltrometer. *Hydrological Sciences Journal* **61** (7), 1263–1279. https://doi.org/10.1080/02626667.2015.1031758.

Salas, J. D. 1980 *Applied Modeling of Hydrologic Time Series*. Water Resources Publication, Littleton, CO, USA. https://books.google.fr/books?id=GinL-8Cc6QgC

Saleh, F., Ducharne, A., Flipo, N., Oudin, L. & Ledoux, E. 2013 Impact of river bed morphology on discharge and water levels simulated by a 1D Saint-Venant hydraulic model at regional scale. *Journal of Hydrology* **476**, 169–177. https://doi.org/10.1016/j.jhydrol.2012.10.027.

Sassolas-Serrayet, T., Cattin, R. & Ferry, M. 2018 The shape of watersheds. *Nature Communications* **9** (1), 3791. https://doi.org/10.1038/s41467-018-06210-4.

Saulnier, G., Beven, K. & Obled, C. 1997 Including spatially variable effective soil depths in TOPMODEL. *Journal of Hydrology* **202** (1–4), 158–172. https://doi.org/10.1016/S0022-1694(97)00059-0.

Sokolovsky, D. L. 1949 Methods of plotting of storm runoff hydrograph by precipitation data. Proceedings of the State Hydrological Institute, Outcome, 14.

Sokolovsky, D. L. 1959 *River Runoff. Hydrometeorological Publishing House*.

Sokolovsky, D. L. & Shiklomanov, I. A. 1969 Estimation of floods with the aid of analogue computers. In: *The Use of Analog and Digital Computers in Hydrology: L'Utilisation des Calculatrices Analogiques et des Ordinateurs en Hydrologie* (IASH/AIHS-Unesco ed). UNESCO – IASH, Tucson, AZ, USA, pp. 87–94. http://hydrologie.org/redbooks/a080/iahs_080_0087.pdf

Strahler, A. N. 1957 Quantitative analysis of watershed geomorphology. *Eos, Transactions American Geophysical Union* **38** (6), 913–920. https://doi.org/10.1029/TR038i006p00913.

Tehrany, M. S., Jones, S. & Shabani, F. 2019 Identifying the essential flood conditioning factors for flood prone area mapping using machine learning techniques. *Catena* **175**, 174–192. https://doi.org/10.1016/j.catena.2018.12.011.

U.S. Department of Agriculture and Natural Resources Conservation Service 2010 *National Engineering Handbook, Part 630 Hydrology, Chapter 15 Time of Concentration*. Washington, DC. https://directives.sc.egov.usda.gov/OpenNonWebContent.aspx?content=27002.wba

USGS – NWIS 2001 *United States Geological Survey – National Water Information System*. https://waterdata.usgs.gov/nwis/rt

Vincendon, B., Ducrocq, V., Saulnier, G. M., Bouilloud, L., Chancibault, K., Habets, F. & Noilhan, J. 2010 Benefit of coupling the ISBA land surface model with a TOPMODEL hydrological model version dedicated to Mediterranean flash-floods. *Journal of Hydrology* **394** (1–2), 256–266. https://doi.org/10.1016/j.jhydrol.2010.04.012.

WaterNSW 2014 *Water New South Wales*. WaterNSW, Australia. https://realtimedata.waternsw.com.au

Xu, C.-Y., Xiong, L. & Singh, V. P. 2019 Black-Box hydrological models. In: *Handbook of Hydrometeorological Ensemble Forecasting* (Q. Duan, F. Pappenberg, A. Wood, H. L. Cloke & J. C. Schaake, eds). Springer, Berlin Heidelberg, Germany, pp. 341–387. https://doi.org/10.1007/978-3-642-39925-1_21.

Yamasaki, K. & Ogawa, H. 1993 A theory of over-learning in the presence of noise. In: *IEEE International Conference on Neural Networks*, San Francisco, CA, USA, pp. 485–488. https://doi.org/10.1109/ICNN.1993.298605

First received 1 December 2019; accepted in revised form 6 February 2020. Available online 15 April 2020